Icarus 363 (2021) 114429

Contents lists available at ScienceDirect

Icarus

journal homepage: www.elsevier.com/locate/icarus

Research Paper

Characterizing landing site safety on Venus using Venera panoramas and Magellan radar properties☆

J. Rabinovitch [*,1], K.M. Stack

Jet Propulsion Laboratory, California Institute of Technology, Pasadena, CA 91109, USA

ARTICLE INFO

Keywords:
Venus
Lander
Radar
Magellan
Venera

ABSTRACT

This study explores an approach for identifying and characterizing sites on Venus where a future lander mission could attain a high probability of safe landing through a synthesis of Venera surface panoramas, Magellan radar properties, and existing global geological maps of the Venus surface. Surface panoramas from the Venera 9 and Venera 13 landers were used to define rock size distributions and to calculate the probability of a hazardous rock encounter for a reference Venus lander design at these specific landing sites. This surface analysis formed the basis and rationale for the development of a set of global filters seeking to identify "safe" 150-km-diameter landing ellipses with Magellan radiophysical properties including root mean square slope, radar backscatter coefficient, and emissivity values similar to the most benign regional plains unit (rp_2) mapped by Ivanov and Head [2011] within the Venera 13 landing site. Using this method, 178 unique ellipses for which >95% of pixels exhibited rms slope and radar backscatter coefficient values similar to the Venera 13 rp_2 unit were identified across the Venus surface. Of these ellipses, 36 also contained >95% of pixels with similar emissivity values as the Venera 13 rp_2 unit. "Safe" ellipses identified by this method were predominantly composed of regional plains, shield plains, and smooth plains as defined in the Venus global geologic map of Ivanov and Head [2011]. Although the method developed in this study for identifying and characterizing safe landing sites on Venus requires several assumptions regarding the correlation of orbiter radar data to surface properties relevant to lander safety, this approach provides a best effort starting point integrating available data for the systematic, relatively objective, and automatic identification of safe landing sites on Venus.

1. Introduction

Robustly designing and successfully delivering a mission to the surface of a planetary body requires knowledge of surface winds, local surface roughness, slope, and the size distribution of hazards at scales relevant to the size of the spacecraft. This information is well known for potential landing sites on Mars, where three decades of orbiter, rover, and lander exploration have contributed to a detailed understanding of the martian atmosphere and surface. The abundance of high-resolution image and topographic data for Mars has also led to the development and verification of methods for assessing landing site safety down to the sub-meter spatial scale (Golombek et al., 2012 and references within; Vasavada et al., 2012). Such analyses, and each successful Mars mission landing that has resulted, have substantially increased confidence in space agencies' abilities to successfully and safely land missions on the surface of Mars.

In contrast to Mars, Venus presents a particularly challenging target for planetary exploration. Surface temperatures of ~460°C and expected surface pressures of ~92 bar (Seiff et al., 1985) require robust spacecraft flight and landing systems. Furthermore, the relatively low spatial resolution and wavelength limitations of existing Venus image datasets largely preclude landing site assessment at the scale and certainty developed for Mars surface missions. For the foreseeable future, potential Venus missions will have to rely on ~100 m/pixel radar data from the Magellan spacecraft (Saunders et al., 1992) to select and evaluate landing sites. In addition, a surface terrain assessment similar to those used to evaluate Mars landing sites is only possible for the landing sites of the Venera 9, 10, 13, and 14 landers, where panorama photographs of

* Corresponding author at: Stevens Institute of Technology, 1 Castle Point on Hudson, Hoboken, NJ 07030-5991, USA.
E-mail address: jrabinov@stevens.edu (J. Rabinovitch).
[1] Work performed while J. Rabinovitch was at the Jet Propulsion Laboratory, California Institute of Technology. Current affiliation is Stevens Institute of Technology, Hoboken, NJ, 07030, USA.

https://doi.org/10.1016/j.icarus.2021.114429
Received 25 May 2020; Received in revised form 6 March 2021; Accepted 8 March 2021
Available online 26 March 2021

the surrounding surface terrain permit measurements of rock distribution and slope on a scale relevant to a landed spacecraft. Despite these challenges, future missions to the surface of Venus will likely result in groundbreaking scientific discoveries regarding the evolution of the interior, surface, and atmosphere of Venus. Accordingly, there has been a strong push for Venus lander mission concepts in the Planetary Science Decadal Survey, reports by the Venus Exploration Analysis Group (O'Rourke et al., 2019), and in the advanced phases of competed mission opportunities (e.g., Hensley et al., 2016; Esposito, 2017; Garvin et al., 2020; Helbert et al., 2020).

Promisingly, previous work has established a possible correlation between surface roughness observed on a regional scale with Pioneer Venus orbiter radar data (>100 km/pixel scale) (Pettengill et al., 1979) and surface roughness observed locally in the Venera surface panoramas (Garvin and Head, 1983), even though there is uncertainty of order hundreds of kilometers in the exact landed location of each Venera spacecraft (Weitz and Basilevsky, 1993). Therefore, although in-situ surface observations for Venus are limited, it may be possible to define criteria for safe landing sites that integrate orbiter data and the few existing in-situ surface observations of the Venus surface for future landed missions until the availability and acquisition of high-resolution radar data analogous to orbiter image and topographic datasets for Mars.

This study explores methods for identifying and characterizing sites on Venus where a lander could attain a high probability of safe landing through a synthesis of Venera surface panoramas, surface properties derived from Magellan radar data, and published global geological maps of Venus. A final landing site for any future Venus mission will have to balance both scientific objectives and engineering safety, but this work focuses primarily on landing safety and the methods by which confidence in safely landing on Venus could be increased. The paper first re-examines rock distribution calculations based on Venera 9 and Venera 13 landing site panoramas, then integrates Magellan orbiter radar data and existing geological mapping efforts to identify and characterize the safety of potential landing sites.

2. Background

Exploration of Venus by robotic spacecraft began in the early 1960s with the successful flyby of NASA's Mariner 2 spacecraft. The late 1960s and early 1970s saw the continued success of the Mariner flybys of Venus and the beginning of the Soviet Venera program. Paired Venera orbiter and lander missions began in 1975 with Venera 9 and 10, which landed at the margin of the Beta Regio area of Venus (Florensky et al., 1977; Weitz and Basilevsky, 1993) (Fig. 1). These missions were followed by the Pioneer Venus orbiter and multiprobes and Venera 11–16 missions in the late 1970s and early 1980s, with the Venera 13 and 14 surface missions landing on the Navka plains west of Phoebe Regio (Fig. 1) and east of the earlier Venera 8 atmospheric probe (Weitz and Basilevsky, 1993). The VEGA 1 and 2 missions to Rusalka Planitia followed in 1984. Since then, NASA's Magellan (1990–1994), ESA's Venus Express (2006–2014), and JAXA's Akatsuki (2010-present) orbiters have all contributed substantially to a better understanding of the Venus surface, atmosphere, and climate, although no missions have been sent to the surface of Venus since the conclusion of the Venera program in the early 1980s. Synthetic aperture radar instruments onboard Venera 15 and 16, Pioneer Venus, and most notably Magellan, the latter of which mapped 98% of the Venus surface at ~100 m/pixel resolution, were revolutionary in advancing understanding of the geology and surface properties of Venus.

2.1. Radiophysical properties of the Venus surface

In the absence of rover, lander, and orbiter image and topographic datasets for Venus analogous to those that exist for Mars, what is known about the surface of Venus beyond the Venera lander sites comes from earth-based telescopic radar observations of Venus (e.g., Campbell and Campbell, 1992; Carter et al., 2006; Kratter et al., 2007), Venus orbiter radar data, and comparisons to radar observations of Earth analog landforms and surfaces (e.g., Ivanov et al., 2017b). The radar systems that have been used to observe the surface of Venus have provided measurements of radiophysical properties including radar backscatter cross-section (coefficient), slope, emissivity, and reflectivity, with backscatter cross-section, slope, and emissivity most commonly used to determine surface roughness (Tyler et al., 1991; Campbell and Campbell, 1992; Campbell and Rogers, 1994).

The amount of radar backscatter reflected from a surface depends on the incidence angle of the transmitted electromagnetic waves, the wavelength and polarization of this energy, the roughness of the surface, and the dielectric properties of materials at the surface. In general, when a surface is rough at the wavelength scale of the transmitted energy, radiation is scattered in many directions, including back toward the sensor, resulting in increased radar backscatter and a brighter appearance in radar images. When a surface is smooth at the wavelength scale, radiation is more likely to be scattered away from the sensor resulting in low detected backscatter and a darker appearance in radar images. Radar backscatter return is also influenced by incidence angle, with backscatter decreasing with increasing incidence angle (Ulaby et al., 1982; Campbell and Campbell, 1992). A surface with a high dielectric constant will be a strong reflector and will result in high radar backscatter; surfaces with low dielectric constants are poor reflectors and result in lower radar backscatter.

Rms slope quantifies surface roughness and is defined as the rms difference in height between points separated by a set distance divided by that step size and is commonly reported in degrees (Shepard et al., 2001). Emissivity, the measure of how well a surface approximates a blackbody, is primarily related to the dielectric constant of a material but is also affected by surface roughness and incidence angle (Campbell and Rogers, 1994). If the dielectric properties of a surface vary little, observed differences in emissivity can be directly related to fine-scale surface roughness, with areas of the Venus surface with higher emissivity values tending to be rougher than those with lower emissivity values (Ford et al., 1993). Studies of widespread radar dark parabolic deposits on Venus have also shown the strong influence of mantling deposits, likely related to impact ejecta, on observed scattering and emission properties (Campbell et al., 1992; Bondarenko and Head, 2004; Carter et al., 2004). Bondarenko and Head [2004] showed that the presence of a smooth mantle can lower the radar backscatter and emissivity of a surface, but if the mantle is thin, does not significantly smooth the surface at the wavelength scale of the radar system. This effect can result in surfaces that appear radar dark yet retain roughness at the scale of radar wavelength.

Fresnel reflectivity measures the efficiency of a surface at reflecting electromagnetic radiation, and is also dominantly related to the dielectric properties of the surface material. Rough surfaces will return a weaker signal to the detector as a result of scattering, thus, appearing to have a lower reflectivity than a smooth surface of the same composition if this scattering is not accounted for (Ford et al., 1993).

2.2. Venus landing site analysis

There is little accessible literature discussing the landing site selection process for the Soviet Venera and VEGA missions to Venus, but Basilevsky et al. (2007) attribute the selection of the Venera 8–12 mission landing sites purely to trajectory constraints during optimal launch windows (at Earth-Venus inferior conjunction), as a limited range of Venus longitudes have both Earth- and Sun-visibility during these conjunctions. From Venera 13 onward, radar data was available from the NASA Pioneer Venus mission (Pettengill et al., 1979), which covered 93% of the Venus surface, and could have informed the selection of landing sites based on radar backscatter and trajectory constraints. The VEGA 1 and VEGA 2 spacecraft performed a flyby of comet

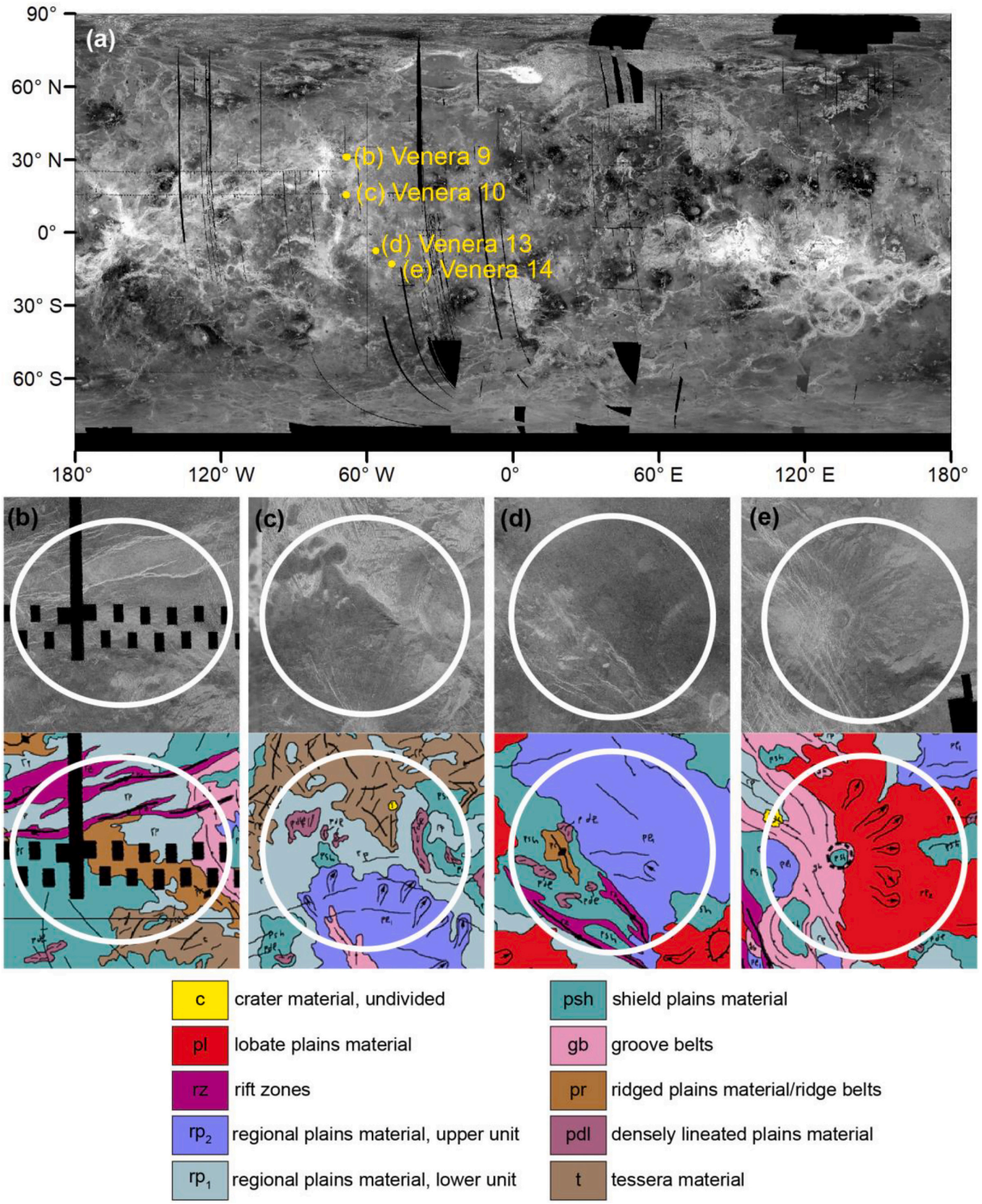

Fig. 1. (a) Landing areas of Venera 9, 10, 13, 14 plotted on the Venus Magellan Global C3-MDIR radar mosaic (Ford et al., 1993). Contrast-enhanced ~100 m/pixel Magellan synthetic aperture radar (SAR) images overlain with the global geologic map of Ivanov and Head (2011) for: (b) Venera 9, (c) Venera 10, (d) Venera 13, (e) Venera 14. The landing areas are delineated as circles 300 km in diameter (Akim and Stepanyantz, 1992).

1P/Halley, which limited where the associated landers could reach on the surface.

The primary geologic characterization of the Venera and VEGA landing ellipses using orbiter radar image data occurred years after completion of the surface missions. Weitz and Basilevsky (1993) and Abdrakhimov and Basilevsky [2002] both produced geologic maps for the Venera and VEGA landing areas, and linked orbiter data sets to surface geology. Although the exact landing sites of the Venera landers are unknown, Weitz and Basilevsky (1993) believed that the Venera landers landed within circular areas with diameters of ~300 km (Fig. 1). Basilevsky et al. (2007) compared the composition and geology of the units identified at the Venera and VEGA landing areas using maps that would ultimately be incorporated into Ivanov and Head's (2011) global geologic map of Venus.

Basilevsky et al. (2007) and Ivanov et al. (2017a) offered candidate landing sites for future Venus landers and possible Venus sample return missions. Basilevsky et al. (2007) focused primarily on the science potential of different geologic units as potential future landing site targets, cautioning avoidance of regions of the Venus surface falling within radar dark parabolic deposits interpreted to be airfall crater ejecta deposits that would obscure pristine, in situ target units. Ivanov et al. (2017b) further identified and characterized potential landing sites for the future Venera-D mission, using comparisons to Earth analogs, extrapolations to regional units mapped on the Venus surface, and scientific potential as the main guide in landing site evaluation. Ivanov et al. (2017b) used the Ivanov and Head (2011) global geologic map for Venus as the foundation for the landing site selection for the proposed Venera-D mission. Ivanov et al. (2017b) evaluated the safety of several of the highest science priority geologic units of the 13 mapped by Ivanov and Head (2011) using radar observations of Earth analogue terrains to determine lander-scale slopes (Ivanov et al., 2017a) for the units, and to assign a "danger rank" of 1–3. This safety evaluation was coupled with scientific potential and priority for exploration to define the selection criteria for a set of candidate ellipses for the Venera-D mission.

2.3. Landing safety characterization for Mars missions

For direct contrast to Venus landing site characterization and safety assessment, modern landing site safety characterization methods for Mars missions have been proven and refined with each successful Mars landing beginning with Mars Pathfinder, followed by the Spirit and Opportunity Mars Exploration Rover missions, the Phoenix Lander, the Mars Science Laboratory Curiosity rover, and the InSight lander (Golombek and Rapp, 1997; Golombek et al., 1997; Golombek et al., 2003a; Golombek et al., 2012). For a passive surface lander, i.e., one that does not employ active hazard avoidance during descent and landing, rocks and meter-to-decameter-scale slopes pose some of the most serious challenges to a safe landing. Rocks and slopes can cause damage to a spacecraft by way of locally high impact loads, or can result in a spacecraft tipping over during the landing event. Small rocks and low slopes, relative to lander length scales, at a prospective landing site not only increase the chances of a safe landing but can greatly simplify the mechanical design and requirements of a spacecraft and its instruments. To model the likelihood of a safe spacecraft landing, the distribution of local rocks and slopes must be known or assumed. The landing site assessment described by Golombek and Rapp [1997] and Golombek et al. [2003a] for Mars stated that the probability of a lander encountering at least one rock with a diameter d greater than D, where D is arbitrary, is given by:

$$P(d > D) = 1 - exp(-L^{*}exp(-sD)^{*}A), \quad (1)$$

where L and s are constants derived from an exponential model fit to an empirical rock distribution, and A represents the cross-sectional area of the lander. When exponential rock size–frequency distribution models are used for Mars, rocks are generally assumed to be hemispherical (Golombek et al., 2003b).

3. Data and methods

3.1. Analysis of Venera 9 and 13 panoramas

3.1.1. Venera panoramas

The only in-situ views of the Venus surface were acquired by the Venera 9 and 10 landers of the Beta Regio region and by Venera 13 and 14 on the Navka plains, at equatorial latitudes in the planet's western and eastern hemispheres, respectively. Venera 9 and 10 included optical-mechanical scanning panoramic television cameras that were mounted ~0.9 m above the ground (Florensky et al., 1977). The field of view of these panoramas was ~40° x 180° with an angular resolution of ~1/3°, and included the area immediately in front of the lander and swaths to the left and right, extending up to the horizon (Florensky et al., 1977). The camera systems on the Venera 13 and 14 landers improved upon those used for Venera 9 and 10, and featured a higher angular resolution of ~1/5° and red, green, and blue colour filters (Basilevsky et al., 1985).

We chose surface panoramas from Venera 9 and Venera 13 to represent characteristic challenging and "safe" landing sites, respectively, based on the presence of potentially hazardous rocks visible in these scenes (Fig. 2). The Venera 9 panorama was selected to represent relatively challenging terrain due to the abundance of rocks of decimeter-scale height visible in the scene (Fig. 2a). The terrain imaged in the Venera 9 panorama was also the rockiest compared to the landscapes imaged by the other three Venera panoramas. Venera 13 was chosen to represent a "safe" landing site because it is substantially less rocky than Venera 9, but contains enough small, loose rocks in the near field that a rock frequency distribution curve could be constructed. The visible rocks in the Venera 13 surface panorama represent a low-risk factor for most lander designs because of their small size (<10 cm diameter) relative to a ~2 m high Venera/VEGA-like lander. The Venera 10 and 14 panoramas also show very flat, rock-free surfaces that would be considered desirable from a landing safety perspective (Fig. 2b and Fig. 2d). However, the Venera 10 and 14 panoramas contain low-relief exposures of in-place bedrock and so few individual rocks that Eq. (1) cannot be used to make a direct comparison of rock size-frequency distribution between these sites and that of the Venera 9 lander.

The Venera 9 and 13 mosaics used in this study were processed by Don P. Mitchell (www.mentallandscape.com). The raw 6-bit values of the Venera 9 image have been transformed to linear brightness, converted to sRGB standard form, and gaps in the panorama have been filled with an inpainting algorithm. The Venera 13 images have been sharpened and contrast-adjusted compared with the original Soviet images.

3.1.2. Venera rock size-frequency analysis

From Eq. (1), the probability that a lander will set down on a rock with a diameter greater than D, P($d > D$), can be determined. To determine L and s for Venera 9 and 13, rock-fragment diameter data from Fig. 3 of Basilevsky et al. [1985] were digitized and fit with an exponential function (Fig. 3). From this fit, L and s were determined for those rocks at the Venera 9 sites, and separate fits were generated for rocks observed in three distinct regions of the Venera 13 site as defined by Basilevsky et al. [1985]: two nearfield regions (Close Zones) and one farfield region (Distant Zone), which were distinguished based on the presence of distinct populations of clasts within each region, as well as the relative distance from the lander. Calculated L and s values are shown in Table 1.

A cross-sectional area of the lander, A, must be chosen to relate the exponential rock distributions to the probability that a spacecraft will strike a rock of a given height. In this study, we considered a three-legged lander with a circular footprint of diameter 4.0 m and a central, spherical pressure vessel of diameter 1.2 m, matching the dimensions of the lander proposed in the VISAGE New Frontiers mission

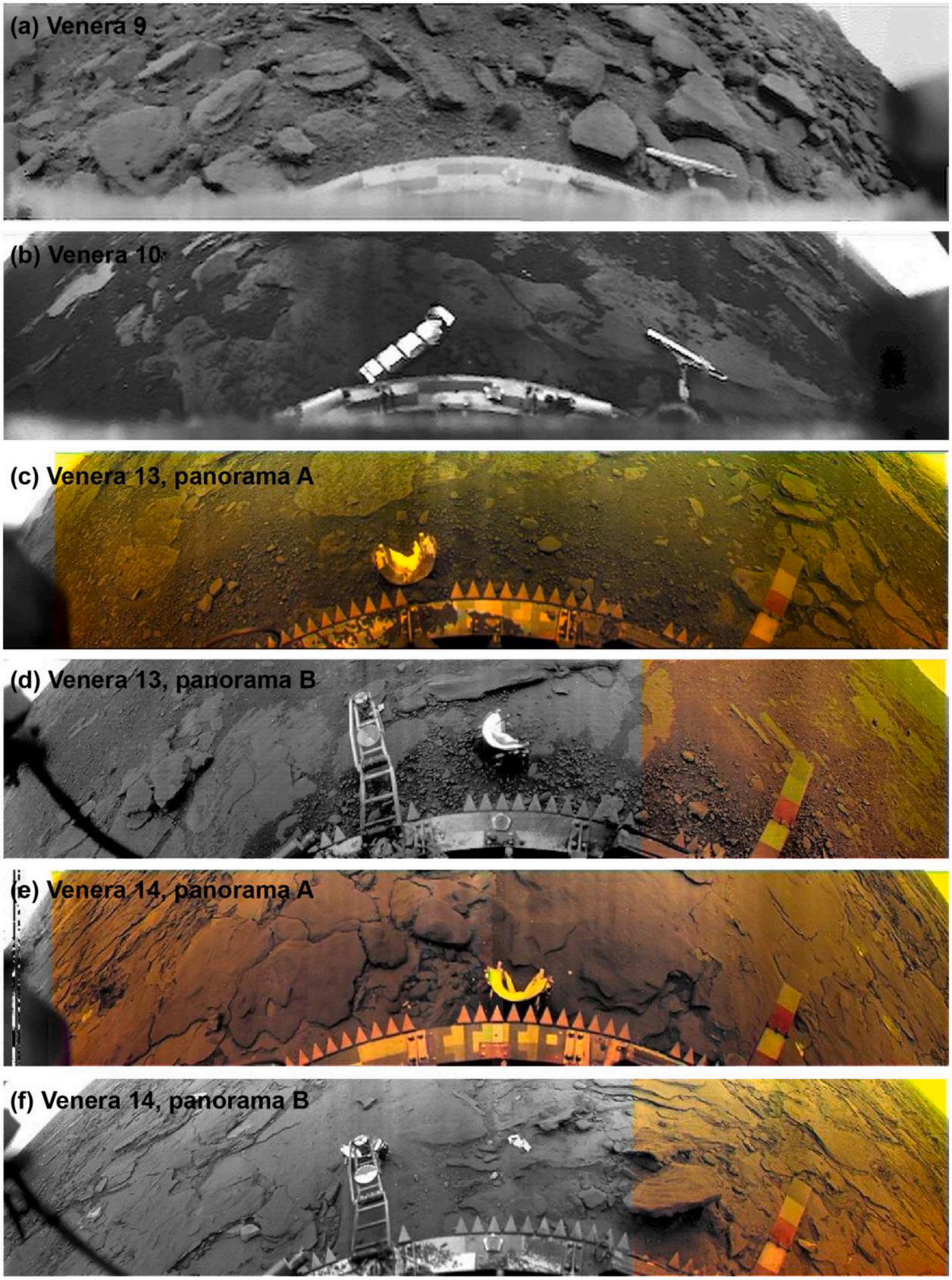

Fig. 2. Surface panoramas acquired by tv cameras on board: (a) Venera 9, (b), Venera 10, (c-d) Venera 13, and (e-f). Panoramas processed by Don P. Mitchell (www.mentallandscape.com).

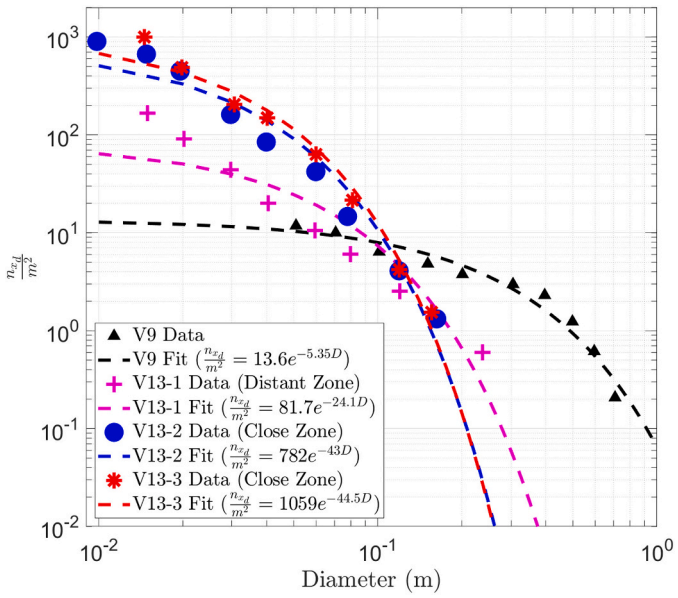

Fig. 3. Rock distributions digitized from Fig. 3 of Basilevsky et al. (1985) and fit with exponential functions. Note that for Venera 13, we created three fits, with one "distant zone" (V13–1) and two "close zones" (V13–2 and V13–3).

Table 1
L and *s* values determined from select rocks at the Venera 9 and 13 landing sites measured by Basilevsky et al. [1985].

Mission	Region	*L*	*s*
Venera 9	All	13.6	5.35
Venera 13	Distant Zone (V13–1)	81.7	24.1
Venera 13	Close Zone (V13–2)	782	43.0
Venera 13	Close Zone (V13–3)	1060	44.5

Fig. 4. A conceptual design for a Venus lander mission concept, showing a central pressure vessel with a ~1.2 m diameter, a leg footprint of diameter ~ 4.0 m, and a rock clearance (post-landing event) of ~0.35 m (vertical clearance between the bottom of the pressure vessel and the ground).

concept (Esposito, 2017) (Fig. 4). The lander's pressure vessel was designed to hold all the required science instruments and avionics at Earth-like temperature and pressure. Therefore, a rock strike to the pressure vessel during landing would have the potential to result in a catastrophic mission failure. This risk motivated the choice of the cross-sectional area of interest for a rock-strike, *A*, to be the area of a 1.2 m diameter circle, which corresponds to the projected cross-sectional area of this reference lander's pressure vessel. Using this area with Eq. 1 allows one to determine the probability that a rock, with a given diameter *D*, will be located below the pressure vessel on the surface during landing. The rock-clearance that a spacecraft has will depend on its mechanical landing design, and therefore every spacecraft and mission may have to use a different value of *D* based on the unique properties of the spacecraft being considered.

To determine a *D*, Golombek et al., 2003a assumed spherical rocks with uniform hemispherical exposures throughout the landing area, the heights of which above the ground were equal to the rocks' radii. To assess this assumption for the Venera 9 and 13 sites, we measured the aspect ratios (height to width) of individual rocks observed in the Venera 9 and 13 surface panoramas (Fig. 5). Only rocks with a cross-sectional edge exposure that enabled an estimation of the rock height were included in the analysis. Two values for the aspect ratio were calculated for each rock: (1) the aspect ratio measured directly from the 2-D panorama; and (2) a conservative aspect ratio based on a correction factor suggested by Golombek and Rapp [1997]. This correction factor is intended to account for the bias that is introduced when using the maximum apparent total width of a rock in a 2D image as the rock's actual width. The actual dimension of a rock shown in a 2D image is a function of the angle at which it is oriented relative to the camera, and Golombek and Rapp [1997] determined that when the length and width of a rock cannot be measured with confidence and its orientation angle is unknown, 0.75 of the apparent maximum width is a reasonable approximation for rock "diameter." Thus, here we calculated conservative aspect ratios using 0.75 of the measured maximum apparent width of each rock under the assumption that the apparent maximum width of the rock we measured was an overestimate of the actual rock width. As the height of a rock that is exposed above the ground is its width multiplied by its aspect ratio, an ideal hemispherical rock would have a measured aspect ratio of 0.5.

We used these newly calculated aspect ratios to derive more realistic rock heights from the measurement of rock diameters made in Basilevsky et al. [1985]. However, Basilevsky et al. [1985] did not discuss their method of measurement, nor the possibility that they may have measured maximum apparent rock width as actual rock diameter, so we conservatively assume that their measurements may overestimate actual rock diameter. Size-frequency distribution models of the probability of encountering a rock of a given height (Golombek and Rapp, 1997; Golombek et al., 2003b) were then calculated for the Venera 9 and 13 landing site panoramas using fits to the rock measurements of Basilevsky et al. [1985], but taking into account the newly measured aspect ratios to determine the likelihood of the VISAGE reference lander striking a rock upon landing (Fig. 6).

3.2. *Magellan analysis*

To identify candidate landing sites across the surface of Venus at which the reference lander described above would have a high probability of a safe and successful landing, a series of global filters were constructed based on Magellan radar characteristics of geologic units mapped by Ivanov and Head (2011) within the Venera 13 landing area. To aid in the definition of the filter bounds, the Magellan radar properties of the Venera 13 landing area were compared to those of the Venera 9 landing area, a site considered more challenging for the safe landing of the VISAGE reference lander.

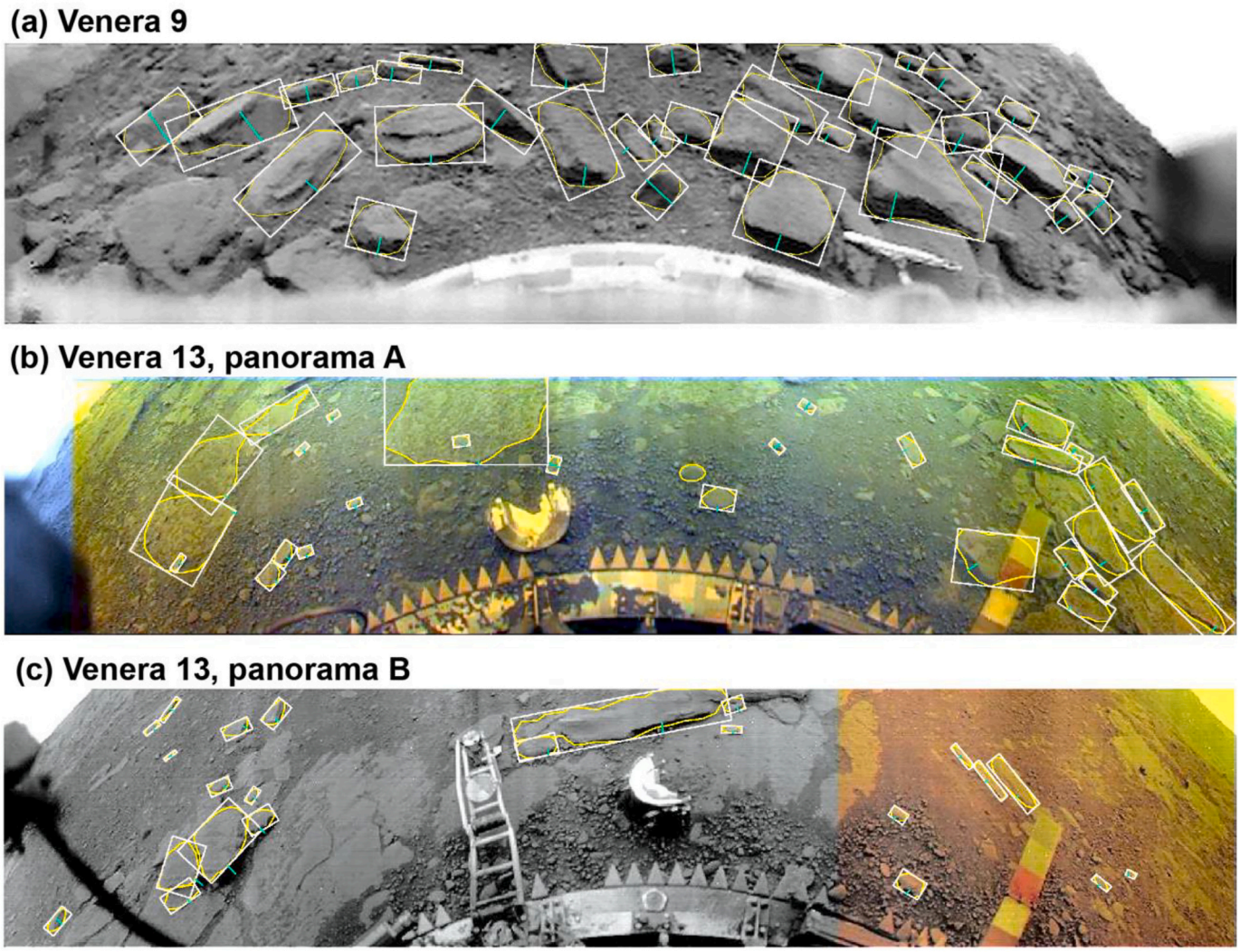

Fig. 5. The Venera 9 and two Venera 13 landing site surface panoramas, annotated to show the blocks (traced in yellow) used to measure aspect ratio. Block diameter was extracted from the length of the white boxes (corrected by a factor 0.75 to account for long axis bias). Approximate block height was extracted from the cyan traces. Only those blocks containing discernible cross-sectional edge exposures were measured. (For interpretation of the references to colour in this figure legend, the reader is referred to the web version of this article.)

3.2.1. Magellan data

The Magellan mission to Venus was launched in May 1989, and operated in orbit around Venus until 1994. Magellan acquired a near-global radar dataset that provides the foundation for identifying possible future landing sites on Venus (Ford et al., 1993). The Magellan sensor acquired synthetic-aperture radar (SAR), altimeter, and radiometer data sequentially in batches by operating in a burst mode (Ford et al., 1993). SAR data was acquired at a wavelength of 12.6 cm, and the radar mapping produced the first global, high-resolution (~100 m) image data set of Venus, covering ~98% of the surface (Saunders et al., 1992). The altimeter was designed to measure the distance between the spacecraft and a patch of the Venus surface approximately 10 to 30 km in diameter (Ford et al., 1993). The radiometry experiment operated in a passive mode and used the high-gain antenna to detect thermal radiation emitted by the Venusian surface (Pettengill et al., 1992).

Radar backscatter for the Venera 9 and 13 landing areas was extracted from the ~75 m/pixel Venus Magellan SAR FMAP Left Look Global Mosaic 75 m v1 (Ford et al., 1993, https://astrogeology.usgs.gov/search/map/Venus/Magellan/Venus_Magellan_LeftLook_mosaic_global_75m). This basemap was also used for qualitative and quantitative assessment of the landing ellipses identified with the global filter (see below). Rms slope and emissivity data were extracted from the Global Slope Data Record (GSDR) and Global Emissivity Data Record (GEDR) data, respectively, (https://astrogeology.usgs.gov/search/map/Venus/Magellan/RadarProperties/Venus_Magellan_MeterScaleSlope_Global_4641m and https://astrogeology.usgs.gov/search/map/Venus/Magellan/RadarProperties/Venus_Magellan_MicrowaveEmissivity_Global_4641m), where pixels for rms slope and emissivity were converted from the original raw 16-bit integers to physical units using the relationships provided in (Ford et al., 1993): DN = (EMISSIVITY * 10000) + 1, and DN = ((SLOPE) * 10) + 1, where DN is the original 16-bit integer value.

In the GSDR basemap, rms slope values were derived from the Magellan altimeter, which measured surface roughness over 10–30 km footprints at scales greater than the radar wavelength (12.6 cm) (Campbell, 1992). Rms slope values reported in the GSDR were calculated by fitting Magellan altimeter echoes as a function of time to Hagfors' radar backscatter models (Ford et al., 1993) and were resampled at a pixel scale of ~5 km by ~5 km (Ford et al., 1993). In the GEDR basemap, values were derived from Magellan radiometer data and that have been corrected for antennae effects and emission and absorption from the Venus atmosphere. Observed emission angle for this data ranged from 48 degrees to 15 degrees off vertical (Ford et al., 1993).

The Magellan Global Reflectivity Data Record (GRDR) (Ford et al.,

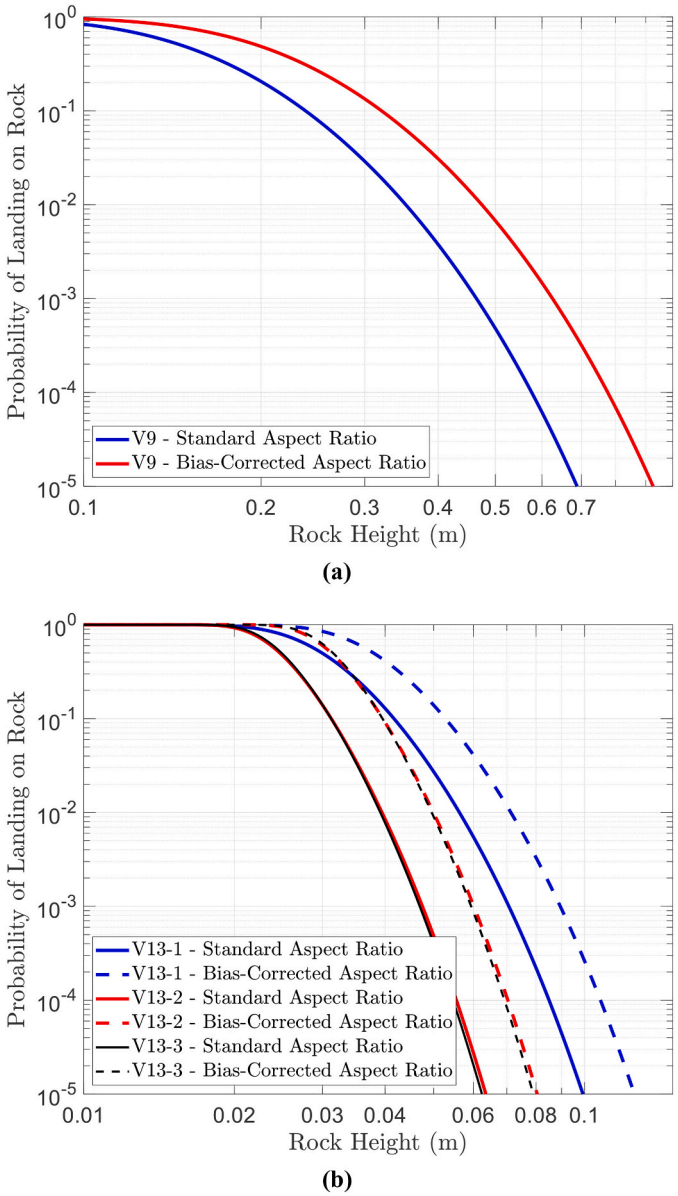

Fig. 6. Calculated probabilities that a ~1.2-m-diameter lander encounters a rock of a given height for Venera 9 (a) and Venera 13 (b). Probabilities are calculated with the as-measured aspect ratios (blue lines) and the bias-corrected aspect ratios (red lines). (For interpretation of the references to colour in this figure legend, the reader is referred to the web version of this article.)

1993) provides Fresnel reflectivity values for much of the surface of Venus. Because the values in the GRDR basemap have been corrected for diffuse scattering, there is minimal surface roughness information contained within the dataset and it was not used in this study.

Extracted emissivity, rms slope, and radar backscatter values plotted in Fig. 7 were used to compare and contrast the radiophysical properties of the Venera 9 and 13 landing areas, and were used to aid in the selection of radar parameters, and their bounding values, the defined the set of global filters employed to identify candidate landing sites on Venus with a high probability of success for the VISAGE reference lander design.

3.2.2. *Magellan orbital data global filter*

To find and characterize other places on the surface of Venus with a probability of safe landing similar to that calculated for the terrain visible in the Venera 13 surface panorama, we first overlaid the ~300-

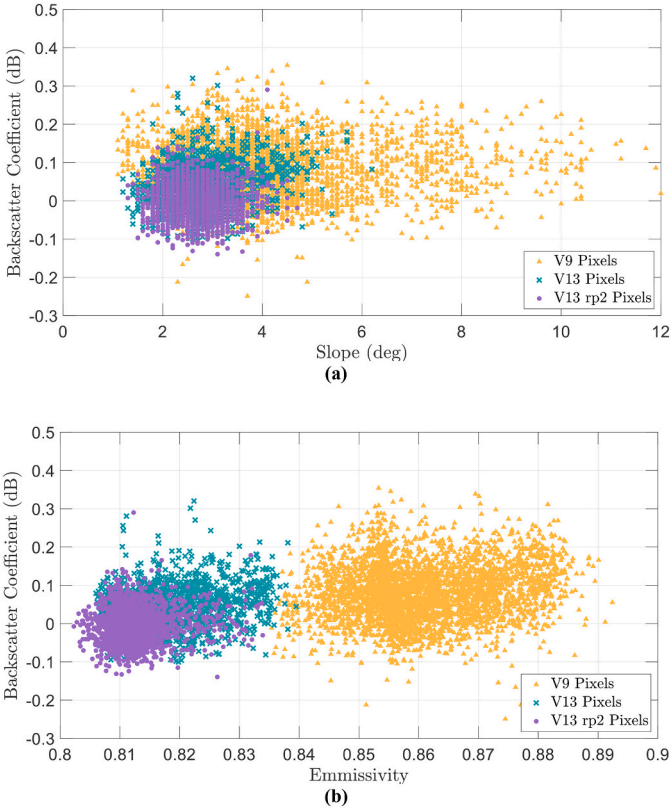

Fig. 7. Plots of (a) SAR backscatter coefficient vs slope and (b) SAR backscatter coefficient vs emissivity, extracted from Magellan radar data for the Venera 9 and Venera 13 landing areas.

km-diameter circle representing the likely Venera 13 landing area from Weitz and Basilevsky (1993) on the Ivanov and Head (2011) global Venus geological map (Fig. 1). Within this landing area, the most extensive unit (>50%) mapped by Ivanov and Head (2011) was "Regional plains, upper unit" (labeled as "rp_2" by Ivanov and Head, 2011). Ivanov and Head (2011) described the rp_2 unit as a "morphologically smooth surface that is moderately deformed by numerous low, narrow, and sinuous wrinkle ridges." The rp_2 unit was also observed by Ivanov and Head (2011) to have a uniform, albeit slightly higher radar backscatter, than the lower member of the plains, rp_1. However, within the Venera 13 landing area, the rp_2 unit exhibits the lowest radar backscatter of the mapped units and exhibits the most featureless terrain as observed in Magellan SAR data.

Because rp_2 is the most extensive unit within the Venera 13 ellipse, we assume that this unit is most readily and reasonably correlative to the terrain observed within the Venera 13 surface panorama, which is considered safe for this study's reference lander design. Abdrakhimov and Basilevsky (2002) made a similar assumption for Venera 13 in their analysis of the geology of the Venera and VEGA landing sites. We recognize that the scale of surface features resolvable in the Magellan radar data is several orders of magnitude larger than those visible within the Venera panorama, and that the distribution of meter-scale and smaller boulders and outcrop exposures in the Venera panorama cannot be directly observed or correlated to the Magellan data. Yet given the limits in spatial resolution of the available radar data for the Venus surface, and that the precise location of Venera 13 within the landing area is unknown, correlating the rp_2 unit, which is relatively bland and featureless in the Magellan SAR data, with the terrain viewed in the Venera 13 panoramas is the conservative and most statistically robust assumption given its predominance within the Venera 13 landing area. By assuming that the terrain present in the Venera 13 panorama is characteristic of the most featureless unit with the lowest radar

backscatter, we accept that a landing site filter defined by the characteristics of the Venera 13 rp_2 unit may exclude characteristics of the other units present within the Venera 13 landing area from being considered "safe."

Following on the assumed correlation of the Venera 13 rp_2 unit with the "safe" terrain visible in the Venera 13 surface panorama, we defined a set of filter bounds that could identify other areas of Venus whose surface characteristics indicated that they were likely to be at least as benign and smooth as the rp_2 unit mapped in the Venera 13 landing area (Table 2). As discussed in the previous section, the terrain observed in the Venera 10 and Venera 14 surface panoramas would also likely be safe from a landing perspective. However, the Venera 13 landing area appears to have less geologic diversity than either the Venera 10 or 14 landing areas observed in Magellan radar images (Weitz and Basilevsky, 1993) (Fig. 1), which, given the large uncertainty in exact landing location for these missions, makes the ground-to-orbiter data comparison for the Venera 13 site more straightforward. In addition, given the latitude of the Venera 9 and Venera 13 landing areas, ~31.01° and −7.55°, respectively, these two sites were observed by Magellan at similar look angles (~42° for Venera 9 and ~ 44° for Venera 13, calculated following the relationship between latitude and look angle shown in (Campbell, 1995, Fig. 1), making a direct comparison of orbiter radar properties from these two locations more robust than a comparison between sites with very different look angles.

Using the Magellan Global Altimetry and Radiometry Records (Ford et al., 1993), we extracted the emissivity and rms slope values for the population of pixels that fell within the portion of the Venera 13 landing area mapped by Ivanov and Head (2011) as rp_2. These extracted values are shown in Fig. 5. Corresponding values of radar backscatter for each pixel in the emissivity and rms slope basemaps were extracted from the 75 m/pixel Magellan SAR FMAP Left Look Global mosaic. Because the SAR basemap is at a higher spatial resolution (~75 m/pixel) than the emissivity and rms slope maps (~4 km/pixel), the SAR value extracted was that corresponding to the center of the corresponding emissivity and rms slope pixels. For comparison to terrains which may be more challenging from a landing perspective, rms slope, emissivity, and radar backscatter were also extracted for all other non-rp_2 pixels falling within the Venera 13 and Venera 9 landing areas. Given that multiple geologic units were mapped by Ivanov and Head (2011) within the Venera 9 landing area (reproduced here in Fig. 1b), we did not attempt to relate the terrain imaged by the Venera 9 panorama to any one particular unit, instead opting to extract radar parameters for the entire landing area. A comparison of the rms slope, emissivity, radar backscatter values for Venera 13 rp_2, all other non-rp_2 Venera 13 units, and Venera 9 can be found in Fig. 7. Values extracted for these landing areas were used to define the bounds of the global filter set described below (Table 2).

To identify candidate safe landing sites with radiophysical properties similar to Venera 13 rp_2, we first ran a global filter to identify terrains between +60 and − 60 degrees latitude with rms slope values ≤5 degrees, the maximum value for rms slope observed within the Venera 13 rp_2 unit (Fig. 8a). We restricted this filter, as well as the SAR backscatter and emissivity filters to this latitude range because the resolution of the emissivity data is poor at higher latitudes (Bondarenko and Head, 2004). We then identified the location of non-overlapping 150-km-diameter ellipses in which ≥95% of the pixels within the ellipse contained rms slope values ≤5 degrees (Fig. 8b). Ellipses passing the rms slope filter then passed the SAR backscatter filter if at least 95% of pixels within a given ellipse exhibited backscatter coefficient values less than or equal to the mean backscatter value of the Venera 13 terrain mapped as rp_2 (Table 2, Fig. 9a). Those ellipses containing at least 95% of pixels whose emissivity values were between the minimum and maximum emissivity values observed for the Venera 13 rp2 unit were considered to pass the emissivity filter (Fig. 9b). 150 km was chosen as the ellipse diameter used to represent a characteristic landing ellipse size for modern Venus missions, which assumes uncertainties associated with: entry flight path angle, vehicle aerodynamics, a ~60 min descent time, and wind distributions provided by VenusGRAM [https://software.nasa.gov/software/MFS-32314-1].

Ellipses were successively and intentionally filtered in this order with rms slope first because it was the least restrictive filter with a clear link to surface features relevant to lander safety. Although radar backscatter was more restrictive than emissivity, the backscatter filter was run after the rms slope filter because it has a recognized and relatively straightforward link to surface roughness, i.e., high backscatter is generally associated with rougher surfaces. Given that emissivity is also sensitive to composition and the presence of low-density surface mantles (e.g., Campbell et al., 1992; Carter et al., 2004; Bondarenko and Head, 2004) it was run as the third filter given the uncertainty in the connection between emissivity values and surface roughness characteristics relevant to lander safety.

To account for the effect of look angle on the radar-derived parameters used to construct the global filters, and to identify those ellipses most directly comparable to the "safe" Venera 13 rp_2 terrain, ellipses passing the SAR backscatter and emissivity filters were further down-selected to those located within the latitude range (−19° to 37°) associated with look angles of +/− 5 degrees within the look angle associated with the Venera 13 area (latitude = −7.55°, look angle = 44°) (Fig. 9). This look angle range was selected following the precedent established by Campbell and Campbell [1992] in their comparison of radar derived parameters of the Venus surface, including emissivity. Ellipses passing the global filters were also compared to the modeled distribution of radar dark parabolic low-density crater ejecta deposits mapped by Basilevsky et al. (2007) (Fig. 10).

The utility and efficacy of this method relies on several assumptions: (1) that the landscape observed within the Venera 13 panorama is generally representative of the rp_2 unit that comprises the majority of the Venera 13 landing circle, (2) that low rms slope, radar backscatter, and emissivity values are generally suggestive of smoother surfaces with minimal hazards at a scale relevant to the landing safety of the VISAGE reference lander, and (3) that the radiophysical properties of Venera 13 rp_2, where observed elsewhere on Venus, also represents surface terrain like that observed in the Venera 13 panorama. The appropriateness of these assumptions will be explored in detail below.

4. Results

4.1. Rock distribution calculations based on Venera 9 and Venera 13 surface panoramas

The average aspect ratio of 33 blocks measured in the Venera 9 panorama (Fig. 5) is 0.26. Applying the correction factor suggested by Golombek and Rapp [1997] to account for long axis bias resulted in an average aspect ratio of 0.35. The average aspect ratio of 53 blocks measured in the Venera 13 panoramas (Fig. 5) is 0.15 (0.19 corrected for long-axis bias). These aspect ratios reflect the predominance of tabular rather than spherical rock fragments observable in the panoramas.

Table 2
Comparison of Magellan radar data-derived surface properties for the Venera 9 and Venera 13 landing areas.

Area	Emissivity range	Emissivity mean	Rms slope range	Rms slope mean	Backscatter coefficient (dB) range	Backscatter coefficient (dB) mean
V13 (rp_2)	0.80–0.83	0.81	1.3–4.7	2.7	−0.14-0.29	−0.0034
V13 (not rp_2)	0.81–0.84	0.82	1.2–6.2	2.8	−0.10-0.32	0.043
V9	0.84–0.89	0.86	1.1–12	4.1	−0.41-0.35	0.075

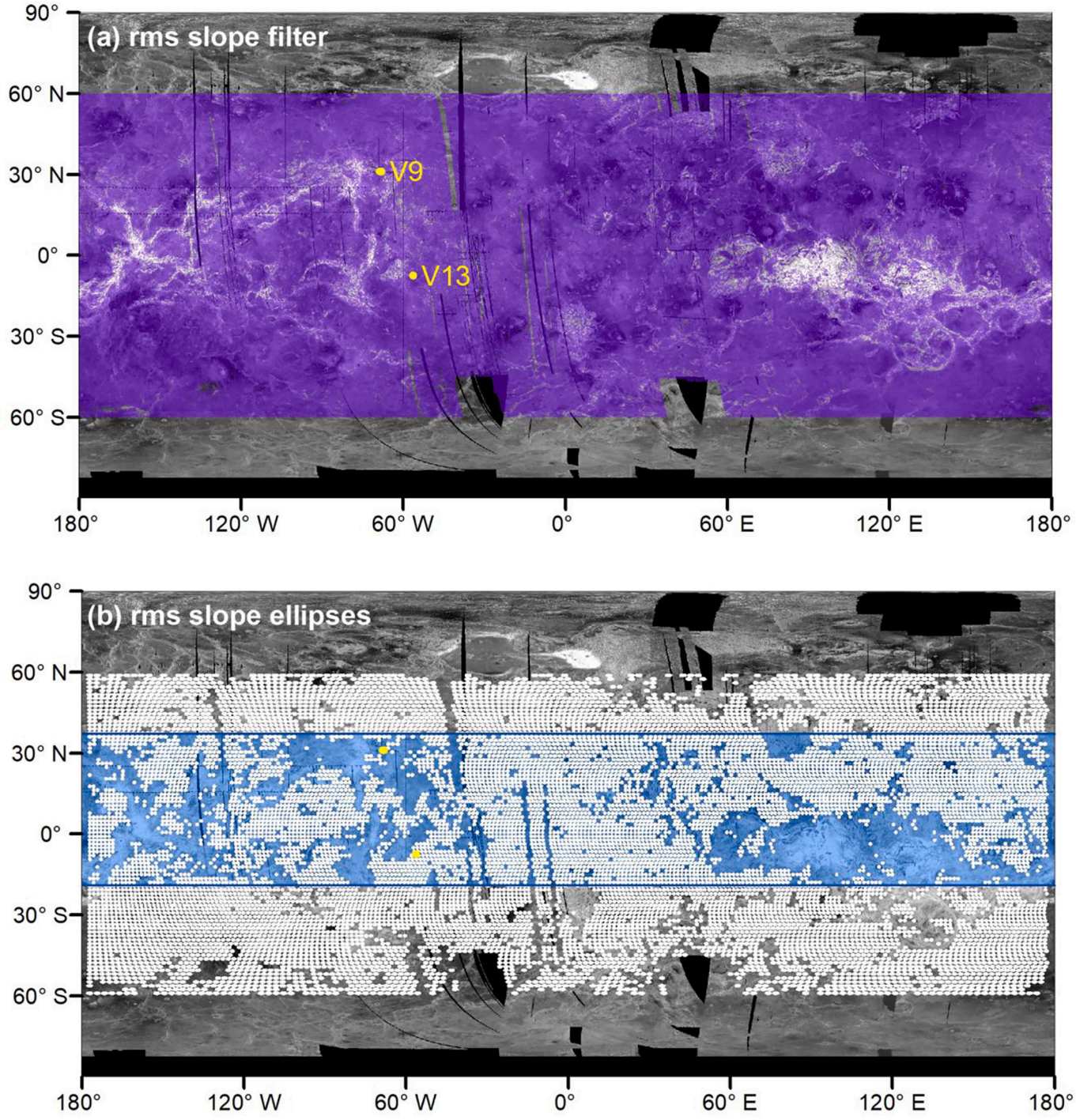

Fig. 8. (a) Areas of the Venus surface (in purple) between 60°S and 60°N whose rms slope values are less than or equal to 5^0. (b) 150-km-diameter ellipses containing at least 95% of pixels with rms slope values less than or equal to 5°. Area highlight in blue is the latitude range (19°S to 37°N) within which ellipse look angle is +/− 5° of the look angle for the Venera 13 ellipse. Yellow ellipses represent the Venera 9 and 13 landing areas. Basemap is the Venus Magellan Global C3-MDIR radar mosaic (Ford et al., 1993). (For interpretation of the references to colour in this figure legend, the reader is referred to the web version of this article.)

Following the method described in Sec. 3.1.2, Fig. 6 shows the probability of a Venus lander encountering a potentially damaging rock given the rock size frequency distributions measured from the Venera 9 and Venera 13 surface panoramas. For conservatism, the worst-case fit from Venera 13 was used to extract rock values for prospective landing sites generally. For example, the plots in Fig. 6 suggest that there is a 0.1% chance that a 1.2-m-diameter lander will encounter a rock with a height of 0.6 m based on the bias-corrected Venera 9 rock distribution. However, that height drops to ~0.09 m for the same percent chance of encounter (0.1%) calculated for the bias-corrected aspect ratio for rocks within the Venera 13–1 zone (see Table 1). The clearance between the surface and the pressure vessel of the VISAGE reference lander design after landing is ~0.3 m. According to the plot in Fig. 6, there would be a negligible chance of experiencing a mission-ending rock strike ($D > 0.3$) m with the potential to pierce the reference lander's pressure vessel for the rock distribution observed at the Venera 13 landing site.

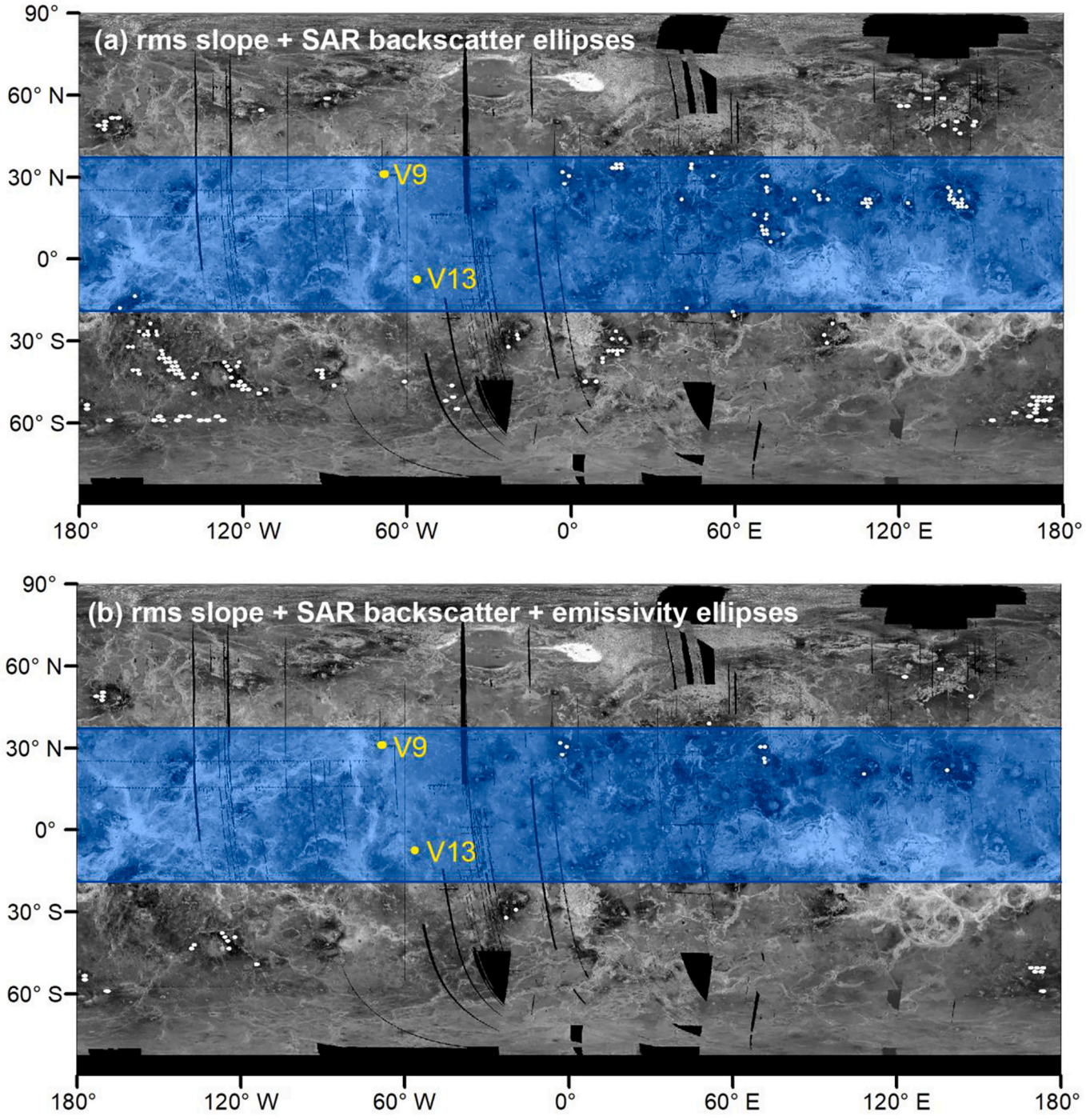

Fig. 9. (a) 150-km-diameter ellipses containing at least 95% of pixels with rms slope values less than or equal to 5° and 95% of pixels with SAR backscatter coefficient values at or below the mean backscatter coefficient calculated for the Venera 13 rp_2 unit. (b) 150-km-diameter ellipses containing at least 95% of pixels with rms slope values less than or equal to 5°, SAR backscatter coefficient values at or below the mean backscatter coefficient calculated for the Venera 13 rp_2 unit, and emissivity values between the minimum and maximum values measured for the Venera 13 rp_2 unit. Area highlight in blue is the latitude range (19°S to 37°N) within which ellipse look angle is +/− 5° of the look angle for the Venera 13 ellipse. Yellow ellipses represent the Venera 9 and 13 landing areas. Basemap is the Venus Magellan Global C3-MDIR radar mosaic (Ford et al., 1993). (For interpretation of the references to colour in this figure legend, the reader is referred to the web version of this article.)

4.2. Global safe-landing filter

The rms slope, emissivity, and SAR backscatter coefficient values extracted from the Venera 13 rp_2 terrain, non-rp_2 areas of the Venera 13 landing area, and the Venera 9 landing area, are shown in Table 2 and in Fig. 7.

The plot in Fig. 7a shows that while there is overlap in the values of rms slope for Venera 13 rp_2, Venera 13 non-rp_2, and Venera 9, the range and mean of rms slope values is greater for Venera 9 than for Venera 13, and the range and mean in rms slope values for the non-rp_2 Venera 13 areas are greater than for the Venera 13 rp_2 unit. Fig. 7a also shows overlap in the values of SAR backscatter coefficient extracted from Venera 9, Venera 13 rp_2, and Venera 13 non-rp_2 terrains, but as for the rms slope values, the variation and mean in backscatter coefficient is

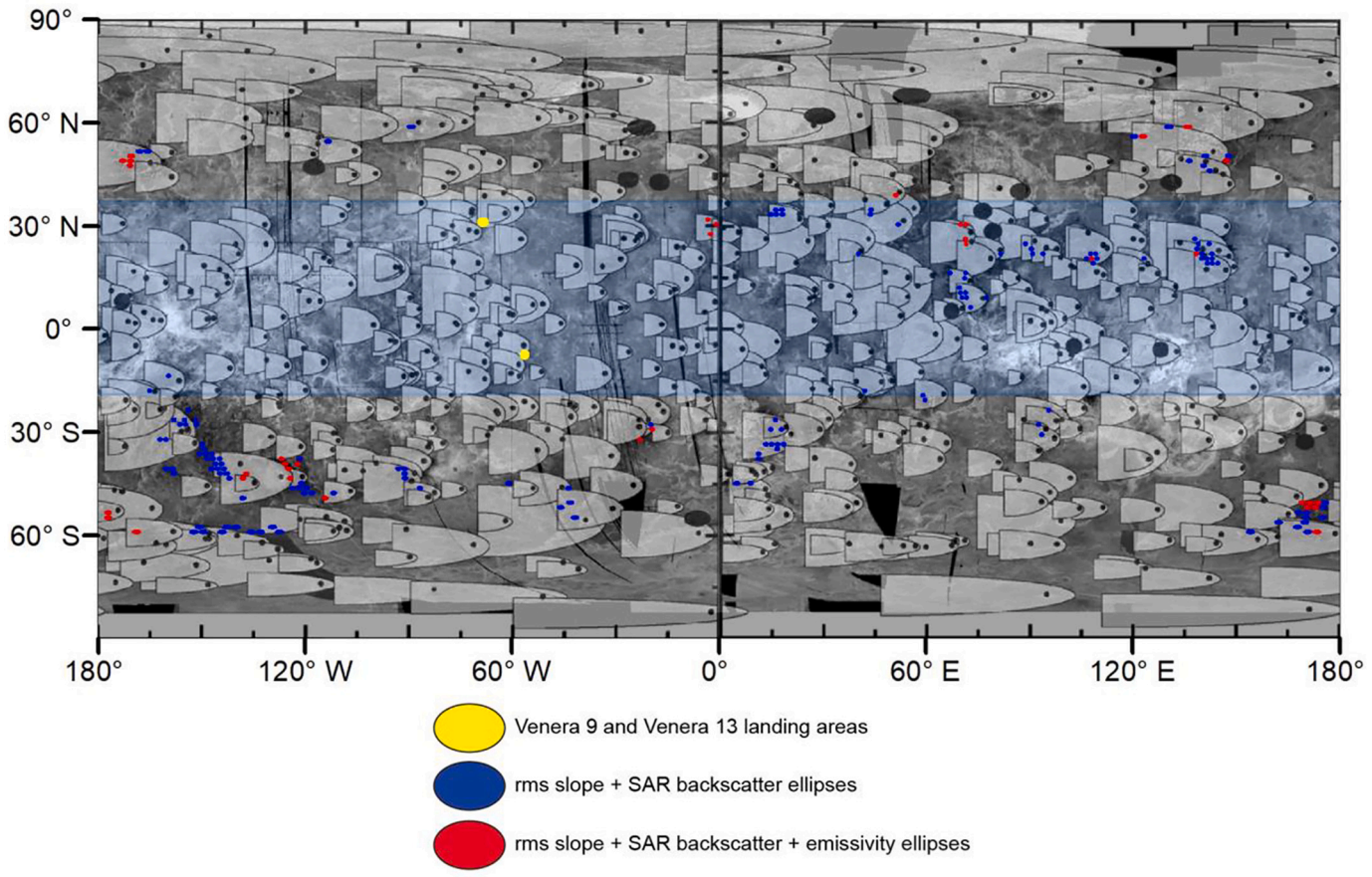

Fig. 10. Venera 9 and 13 landing areas (yellow), ellipses passing the rms slope and SAR backscatter coefficient filters (blue), and ellipses passing the rms slope, SAR backscatter coefficient, and emissivity filters (red) overlain on Basilevsky et al.'s (2007) map of the modeled distribution of radar dark parabola deposits. Black ellipses are those identified by Basilevsky et al. (2007) as candidate Venus landing sites of interest falling largely outside of modeled parabolas. Area highlight in blue is the latitude range (19°S to 37°N) within which ellipse look angle is +/− 5 degrees of the look angle for the Venera 13 ellipse. (For interpretation of the references to colour in this figure legend, the reader is referred to the web version of this article.)

lowest for Venera 13 rp_2 and greatest for the Venera 9 landing area. The difference between the Venera 13 and Venera 9 landing areas is most apparent in the emissivity values plotted in Fig. 7b. The emissivity values for the Venera 13 rp_2 unit and nearly all those extracted from non-rp_2 Venera 13 landing area are distinct from, and are lower than, those extracted from the Venera 9 landing area.

Candidate "safe" ellipses identified by the global filters for rms slope, SAR backscatter coefficient, and emissivity are shown in Figs. 8–9 and listed in Supplementary Tables 1–3. Approximately 92% of the Venus surface between +60 and -60 degrees latitude passed the rms slope filter (rms slope less than or equal to 5 degrees) (Fig. 8a), within which 12,267 non-overlapping, 150-km-diameter ellipses containing at least 95% of pixels with rms slope values less than or equal to 5 degrees (Fig. 8b, Supplementary Table 1). A visual inspection of these ellipses in SAR backscatter revealed that many of the ellipses passing the rms slope filter include terrain that is radar bright (Fig. 11a), or that contain radar bright surface features like rift zones, ridges, and tessera (e.g., Fig. 11b and Fig. 11c). Of the ellipses that passed the first rms slope filter, 178 ellipses passed the much more stringent SAR backscatter filter requiring at least 95% of the pixels within the ellipses to exhibit radar backscatter coefficient values at or below the mean SAR backscatter of the Venera 13 rp_2 unit (Fig. 9a, Supplementary Table 2). Visual inspection of these ellipses showed generally radar dark terrains and near uniform radar backscatter within each ellipse (e.g., Fig. 11d-f). The 178 landing ellipses that passed both the rms slope and SAR backscatter filters predominantly contain terrain mapped as "regional plains material, lower unit" ("rp_1") (Fig. 12a). Additional geologic units identified by Ivanov and Head (2011) found within these ellipses include "lobate plains," "shield plains," "smooth plains," "rp_2," and "shield clusters" (Fig. 12a) These units are relatively featureless and exhibit uniform and relatively low backscatter where they occur within the filtered ellipses. Of the 178 ellipses, 54 are located within the latitude range associated with a +/− 5 degree look angle difference compared to the Venera 13 landing area. A majority of the ellipses passing the rms slope and SAR backscatter coefficient filters are also located within parabolas modeled by Basilevsky et al. (2007) (Fig. 10), although there are 38 ellipses within several clusters located in the southern hemisphere including north of Imdr Regio (~36°S, 149°W), south of Rokapi Dorsa (~58°S, 138°W), north of Tinianavyt Dorsa (~47°S, 120°W), and northeast of Dsonkwa Regio (~53°S, 167°E) that occur outside of modeled dark parabolas (Supplementary Table 2). There are no ellipses that occur within the preferred look angle latitude range and are outside of modeled parabolas.

Of the 178 ellipses that passed the rms slope and backscatter coefficient filters, 36 also passed the emissivity filter, meaning that 95% or more of the pixels contained within the ellipses exhibited emissivity values between the minimum and maximum emissivity values observed within the Venera 13 rp_2 unit (Fig. 9b, Supplementary Table 3). These 36 ellipses are primarily composed of terrain mapped by Ivanov and Head (2011) as "regional plains material, lower unit" ("rp_1"), as well as "smooth plains material," "shield plains material," "regional plains material, upper unit" ("rp_2"), and "lobate plains material" ("pl") (Fig. 12b). The units dominantly present within the 36 ellipses all have in common a generally uniform, radar dark appearance with minimal radar bright features (e.g., Fig. 11g-i). Only 9 of the 36 ellipses that

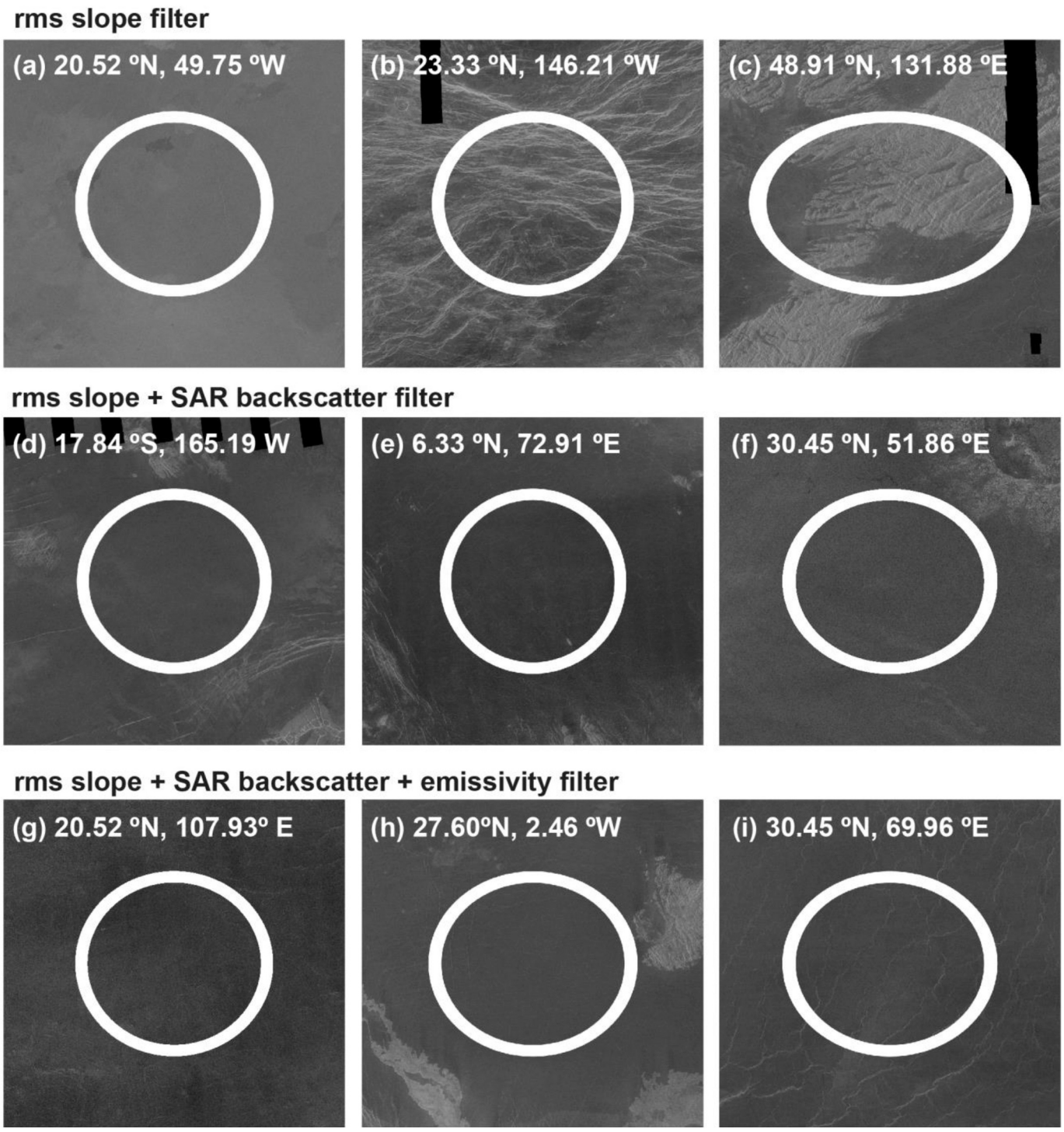

Fig. 11. (a-c) Example 150-km-diameter candidate landing ellipses (outlined in white) that passed the rms slope filter, but not the SAR or emissivity filters. (d-f) Example 150-km-diameter candidate landing ellipses (outlined in white) that passed the rms slope and SAR filters, but not the emissivity filter. These three ellipses also have look angles within +/− 5 degrees of the Venera 13 look angle and occur within modeled parabola deposits. (g-h) Example 150-km-diameter candidate landing ellipses (outlined in white) that passed the rms slope, SAR, and emissivity filters. These three ellipses also have look angles within +/− 5 degrees of the Venera 13 look angle and occur within modeled parabola deposits. All ellipses have been overlain on the ~75 m/pixel Magellan SAR FMAP Left Look Global mosaic (Ford et al., 1993).

passed all three filters are located within the latitude range associated with look angles within +/− 5 degrees of that of the Venera 13 landing area. These 9 ellipses are composed entirely of "rp_1" or "shield plains material." Eight ellipses (including several near Dsonkwa Regio) that also passed the emissivity filter occur outside of modeled parabola deposits, but all others passing the emissivity filter occur within modeled parabolas (Fig. 10, Supplementary Table 3). None of the ellipses occurring outside of modeled parabolas are within the preferred look angle latitude range.

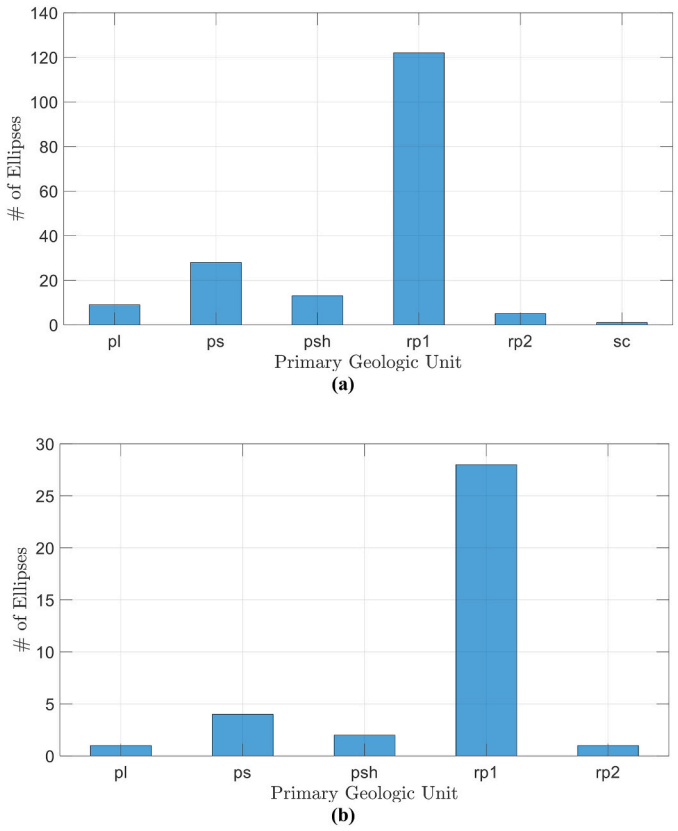

Fig. 12. Histograms showing (a) the frequency of primary geologic units occurring within the ellipses that passed the rms slope and SAR backscatter coefficient filter and (b) the frequency of primary geologic units occurring within the ellipses that passed the rms slope, SAR backscatter coefficient filter, and emissivity filter.

5. Discussion

This study presents a method for identifying potential safe landing sites on Venus using existing orbiter and in-situ data, taking into account observations from the Venera 13 landing site and a reference lander design. Below, we explore comparisons to previously published landing-site assessments for Venus, consider the reasonableness of this study's assumptions, and discuss implications of this work for the identification of future safe landing sites on Venus.

5.1. *Defining "safe" for landing sites on Venus*

For recent Mars missions, acceptable probabilities of successful landing are typically on the order of ~98.5% or greater, with these probabilities being the result of intensive rock counting at the sub-meter scale and sophisticated landing simulations that take into account, among other things, rocks and other hazards (e.g. dust storms), and models of atmospheric conditions (Chen et al., 2017). Confounding questions for future Venus mission proposals remain: how does one define "safe" for a landing ellipse on Venus, and how does one make a convincing case for the high probability of a successful landing?

The results of the probability calculations based on the rock size frequency distribution at the Venera landing sites (Fig. 6) show that there would be a negligible chance of the VISAGE reference lander encountering a mission-ending rock capable of piercing its pressure vessel (>0.3 m in height) in the immediate terrain around the Venera 13 lander. Even though the Venera 9 landing site is significantly rockier than that of Venera 13, the plot in Fig. 6 shows that the probability of encountering a rock taller than 0.3 m is still quite low at <0.2%. Given the near total paucity of blocks in the Venera 10 and 14 panoramas, it is reasonable to assume a very high probability of successful landing at these sites as well. And, indeed, the successful landing of all four Venera missions is proof that these sites, including the more challenging terrain of Venera 9, were "safe enough" landing sites for the Venera spacecraft design.

Thus, the challenge for Venus is not necessarily finding individual locations where a lander could safely touch down on the surface, as the successful landings of the Venera and VEGA landers have shown. Rather, the particular challenges for safe landing on Venus, especially compared to Mars, are the large size of landing ellipses required for missions sent to the Venus surface, and the difficulty of saying with any certainty whether a safe landing on Venus can be guaranteed given the current limitations of orbiter radar data for the Venus surface. This latter point is particularly relevant for proposers of future Venus missions who find themselves in the position of needing to convince funding agencies that a mission has a high-enough probability of landing success.

Landing ellipses on the order of ~150 km in diameter are relevant for Venus given uncertainties in spacecraft entry flight path angle (to begin the entry, descent & landing sequence), uncertainties in atmospheric winds – amplified by the long descent time (~60 min) a spacecraft typically undergoes to reach the surface of Venus due to the high density atmosphere, as well as high-temperature challenges (close to the Venus surface) which make any technologies that could aid a spacecraft target a specific landing site difficult and costly to implement. Thus, it is important not only to identify terrain types on the Venus surface with a high likelihood of a successful and safe landing, but also to identify areas large enough that this likelihood remains reasonably high within a given landing ellipse despite relatively large uncertainties in an exact landing location. For example, the presence of a network of steep-sided ridge or groove belts or a rift zone cutting through an otherwise benign landing ellipse on the regional plains of Venus has the potential to pose mission-ending risks to a lander without the aid of hazard avoidance technology.

Previous studies that have proposed candidate landing sites for future Venus missions have focused primarily on science considerations, e.g., Basilevsky et al. (2007) and Basilevsky et al. [2014], or have performed very general safety assessments for broad geologic units, i.e., Ivanov et al. (2017b) who assigned a danger rank of 1–3 to several high priority geologic units from the Ivanov and Head (2011) global geologic map. Although Ivanov et al. (2017b) proposed several candidate ellipses for the Venera-D mission, the focus of their prioritization was the scientific potential and generic terrain type/geologic unit present at the sites, rather than a detailed assessment of the safety of the proposed sites. Ivanov et al. (2017b), the most in-depth characterization to-date of terrain types as potential Venus landing sites, used Earth analogues to determine that the "smooth plains" of Venus were the safest terrain for landing the Venera-D mission. But Ivanov et al. (2017b) stopped short of identifying specific candidate ellipses on the surface of Venus that met their desired slope characteristics.

While acknowledging the unavoidable limitations in data resolution and the general uncertainties in the interpretation of radar-derived surface properties, in this study we took advantage of the likely correlation between the terrain imaged in the Venera 13 surface panorama and the large area of radar dark, relatively uniform terrain mapped within the Venera landing area as rp_2 to provide the basis for a definition of "safe" terrain on which a lander would have a high probability of landing successfully. It became clear after running the rms slope filter, and visually inspecting a subsample of the ellipses in SAR backscatter images, that the rms slope filter alone was not sufficient for identifying candidate landing sites with a high probability of safe landing given the prevalence of radar bright terrain and structural features within many of the ellipses. That this was the case is not particularly surprising given the relatively low resolution of the rms slope data and the wide variation in scale of roughness (cm- to km-scale) that this dataset conveys. Fortunately, the SAR backscatter filter was very successful at down-selecting ellipses to those with very uniform, relatively low radar backscatter

values. While we chose 95% as the required threshold for pixels within an ellipse exhibiting radar characteristics that matched the filter bound (s), this threshold could be increased or decreased depending on the desired risk tolerance for more-or-less potentially radar bright hazards. The emissivity filter further narrowed down the ellipses but given the potential uncertainties in the relevance of emissivity as it relates to surface roughness, we consider this filter less important for identifying potential safe landing sites on Venus.

Although the method we employed here was largely agnostic to scientific potential and prioritization, the ellipses that passed the SAR backscatter and emissivity filters were predominantly composed of regional plains units (particularly "rp_1"), smooth plains material, and extensive shield or lobate plains units as mapped by Ivanov and Head (2011). Ivanov et al. (2017b) determined that the rp1 and smooth plains units were among the highest priority units for future exploration by Venus surface missions, so the results of this study are fortuitously complementary and consistent with the science and exploration prioritization described by Ivanov et al. (2017b). Tessera terrain, which is often cited as one of the most important targets for future Venus exploration, is almost entirely excluded from this study's set of candidate ellipses given that tessera is generally radar bright. Landing site selection is necessarily a compromise and balance of safety and scientific priorities, but our study's methods provide a relatively objective characterization of safe landing sites that supports and confirms previous qualitative assessments, and is still in line with community scientific priorities.

5.2. Global filter assumptions

Although we consider this study's method for identifying and characterizing safe landing sites on Venus to be generally conservative in identifying "safe" places to land (i.e. this study likely excludes places on the surface of Venus that would be safe to land on), below we consider various factors that may affect the validity and reasonableness of the assumptions and extrapolations we make in this work.

We assume that the distribution of rocks observed in the Venera 13 surface panorama is generally representative of the rock distribution present on the surface throughout all of the terrain mapped as rp_2 within the Venera 13 landing area. Since the rp_2 unit mapped within the Venera 13 landing area appears to be the darkest and most uniform in the SAR radar backscatter images, this assumption seems reasonable and relatively conservative with the caveat that independently verifying that all of the rp_2 unit within the Venera 13 landing area appears similar to the terrain imaged in the Venera 13 surface panorama is simply not possible with the current datasets available for the Venus surface.

The plots presented in Fig. 7 provide some confidence that Magellan radar parameters can be used to distinguish Venera 13-like terrains from areas of the surface that may present a greater challenge for safe landing (e.g., Venera 9 and non-rp_2 regions of the Venera 13 landing area). Although there is some overlap in the rms slope values of Venera 13 rp_2, Venera 13 non-rp_2 terrain, and Venera 9, the slope values for Venera 13 rp_2 all fall below ~5 degrees (Fig. 7a). In contrast, slope values between 5 and 10° are common within the Venera 9 landing area. Fig. 7a also clearly illustrates that SAR backscatter coefficient values for Venera 13 rp_2 are lower, and within a narrower range than those of non-rp_2 Venera 13 or Venera 9 terrain. This pattern observed in the Magellan data, coupled with what we know of the surface from the Venera 13 and Venera 9 lander panoramas supports our assumption that terrains with lower rms slope and radar backscatter are likely to be smoother and more benign. However, we acknowledge that this approach does not account for all potential variations in the material properties of the surface that may affect radar return, or the possibility that surface roughness may be present on a scale not observable in the Magellan data, but still potentially damaging to a lander. The results presented here represent a best effort attempt to use the available data for the Venus surface to identify safe landing sites, but the resolution limitations of the existing Magellan radar data and the uncertainties inherent to correlating radar-derived parameters to meter and sub-meter scale morphological features relevant to lander safety remain significant challenges for this and future analyses of landing site safety.

Fig. 7b shows that emissivity values for the pixels mapped as rp_2 within the Venera 13 ellipse are completely distinct from those representing the Venera 9 landing area. The Venera 13 and Venera 9 landing areas were observed at similar look angles, 44° and 42° respectively, so it is unlikely that variations in look angle can explain the difference in emissivity observed between the landing areas. Differences in composition, however, could explain such a spread. The rocks present at the Venera 9 landing site are generally interpreted to be tholeiitic in composition (Abdrakhimov and Basilevsky, 2002), while those observed at Venera 13 are interpreted to be representative of a more alkaline-rich basalt with significantly enhanced potassium relative to the tholeittic basalts observed at the other Venera and VEGA landing sites (Barsukov et al., 1982; Abdrakhimov and Basilevsky, 2002). Emissivity is also known to be affected by the presence of low-density mantling deposits of variable thickness (Campbell et al., 1992; Carter et al., 2004; Bondarenko and Head, 2004). The Venera 13 landing area is partially within a modeled parabola interpreted as low-density impact ejecta, while the Venera 9 ellipse is entirely within a modeled parabola (Basilevsky et al., 2007) (Fig. 10). The presence of these airfall deposits in and of itself is not necessarily problematic for landing safety as they are likely to be relatively smooth and flat (Basilevsky et al., 2004), but differences in emissivity between the two landing areas could be due to the variable presence and thickness of these mantles rather than a difference in surface roughness. While interpreting differences in emissivity values between the Venera 13 and Venera 9 ellipses is complicated by the potential effect of compositional differences and variable mantling by airfall deposits, the units mapped within Venera 13 shows that the terrain mapped as rp_2 generally exhibits lower emissivity values and a narrower range in values than emissivity values associated with non-rp_2 units mapped within the Venera 13 landing area. The uncertainties associated with the physical interpretation of emissivity values applied to landing safety also motivated the use of a range for the emissivity filter, instead of simply using the maximum emissivity value observed in the rp_2 portion of the Venera 13 landing area as a threshold. Limiting the allowable range of emissivity, while likely filtering out landing ellipses that could be considered safe, attempts to ensure that landing ellipses that pass the emissivity filter are similar to the Venera 13 landing site, and therefore are more likely to have a rock distribution akin to what Venera 13 observed. Still, the results of this study's emissivity filter should be considered with the potential effect of these various factors in mind, and therefore greater weight is placed on the results of the rms slope and SAR filters.

The method presented here undoubtedly misses many areas that would, in reality, be safe landing sites. While conservative and restrictive, the approach presented here has the benefit of providing a clear, relatively objective definition of "safe" terrain based on Venera 13 rp_2 values of rms slope, emissivity, and SAR backscatter coefficient. Furthermore, this method identifies highly uniform, appropriately-sized ellipses in an automated way. Future efforts to identify landing sites on Venus could adjust the bounds of the filters or the percentage threshold to suit the desired risk tolerance.

The global filter we used in this study to identify safe landing sites relied upon the geologic mapping of the Venera 13 landing area by Ivanov and Head (2011), particularly the mapped extent of the rp_2 unit, and upon the placement and area of the Venera 13 landing area proposed by Weitz and Basilevsky (1993). The bounds of the global filter are sensitive to the placement of these boundaries, but by using the mean value of radar backscatter for the filter, and only the maximum values of the rms slope we hoped to minimize the sensitivity on the exact placement of the mapped contacts. The emissivity filter, which uses a range, is likely the most sensitive to the mapped rp_2 boundary in the Venera 13 landing area. Fortunately, while there is subjectivity inherent to the

process of geologic mapping in the identification and definition of units and in the way that contacts are drawn, there is general consistency in the way that the Venera 13 ellipse was mapped by Ivanov and Head (2011), Weitz and Basilevsky (1993), and Abdrakhimov and Basilevsky [2002]. While the global filter bounds used in this work were based upon the characteristics of the rp_2 unit mapped within the Venera 13 landing area, the filters are otherwise agnostic to geologic mapping interpretations for the rest of the Venus surface. Thus, our method has the benefit of being able to identify terrain with "Venera 13-like" radiophysical properties even if they were not mapped originally as rp_2. This was illustrated in the results of the global filter, which identified ellipses containing most commonly "rp1," "lobate plains," "shield plains," and "smooth plains" rather than rp_2 which, outside of the Venera 13 landing area, tends to be brighter and contains a higher proportion of radar bright structural features than the units most commonly found in this study's candidate ellipses. The most abundant unit types found in the filtered ellipses have in common that they were described by Ivanov and Head (2011) as being morphologically smooth, with relatively limited tectonic deformation, especially compared to the radar bright features found within areas of the surface mapped as "tessera," "groove belts," "ridged plains," or "densely lineated terrains." There is a potential drawback to the method employed here in that it specifically filters out some of the most geologically interesting terrains on Venus, such as the "tessera" terrain, and can emphasize ellipses more likely to contain radar-dark parabolic airfall deposits (e.g., Basilevsky et al., 2014). However, if landing safety is the primary concern of a mission, the method presented here, which is largely agnostic to the scientific potential of the landing ellipses selected, is able to select and consistently define a set of landing ellipses with a likely high probably of landing success based on what we know and understand of the radiophysical and surface characteristics of Venera 13 rp_2-like terrain. Future Venus measurements, such as higher resolution SAR data or improved emissivity measurements, could help better characterize the surface and aid in determining where composition is a primary influence on the radar backscatter return; these data could be used to improve the fidelity of the analysis presented in this work.

6. Conclusions

This work reports a method to develop a systematic and objective assessment and selection of "safe" landing sites for future Venus lander missions. Existing surface panoramas from the Venera 9 and 13 landers were used to characterize rock size distributions associated with these specific landing sites. A global filter was defined to identify areas of the Venus surface that are morphologically and radiophysically similar to the Venera 13 landing area. Although necessitating several assumptions regarding radar data, geologic mapping, and surface properties, this approach provides a systematic, relatively objective, and automated method that integrates orbiter and in-situ surface data for identifying safe landing sites on Venus with a high probability of safe landing. In the future, the ellipses presented in this work could be used in conjunction with maps depicting other high scientific priorities for landed surface missions to Venus to ensure that both scientific priorities and engineering constraints can be met.

Declaration of Competing Interest

None.

Acknowledgments

The authors would like to thank Mikhail Ivanov and James Head for providing a digital copy of their Venus geological surface map. The authors would also like to thank Mark Bullock, Jeffrey Plaut, and the VISAGE proposal team for productive conversations related to this work. We thank Paul Byrne and an anonymous reviewer for providing feedback that substantially improved the quality of this manuscript. This research was carried out at the Jet Propulsion Laboratory, California Institute of Technology, under a contract with the National Aeronautics and Space Administration (80NM0018D0004).

Appendix A. Supplementary data

Supplementary data to this article can be found online at https://doi.org/10.1016/j.icarus.2021.114429.

References

Abdrakhimov, A.M., Basilevsky, A.T., 2002. Geology of the Venera and Vega landing-site regions. Sol. Syst. Res. 36 (2), 136–159.
Akim, E.L., Stepanyantz, V.A., 1992. Landing sites of automatic interplanetary probes on new map of Venus (in Russian). Astron. Vestn.
Barsukov, V.L., Volkov, V.P., Khodakovsky, I.L., 1982. The crust of Venus: theoretical models of chemical and mineral composition. J. Geophys. Res. Solid Earth 87 (S01), A3–A9.
Basilevsky, A., Kuzmin, R., Nikolaeva, O., Pronin, A., Ronca, L., Avduevsky, V., Uspensky, G., Cheremukhina, Z., Semenchenko, V., Ladygin, V., 1985. The surface of Venus as revealed by the Venera landings: part II. Geol. Soc. Am. Bull. 96 (1), 137–144.
Basilevsky, A.T., Head, J.W., Abdrakhimov, A.M., 2004. Impact crater air fall deposits on the surface of Venus: areal distribution, estimated thickness, recognition in surface panoramas, and implications for provenance of sampled surface materials. J. Geophys. Res. Planet 109 (E12).
Basilevsky, A.T., Ivanov, M.A., Head, J.W., Aittola, M., Raitala, J., 2007. Landing on Venus: past and future. Planet. Space Sci. 55 (14), 2097–2112. ISSN 0032-0633. https://doi.org/10.1016/j.pss.2007.09.005.
Basilevsky, A.T., Ivanov, M.A., Head, J.W., 2014, May. Potential landing sites for future missions to Venus. In: Workshop on Venus Exploration Targets, Vol. 1781, p. 6032.
Bondarenko, N.V., Head, J.W., 2004. Radar-dark impact crater–related parabolas on Venus: characterization of deposits with Magellan emissivity data. J. Geophys. Res. Planet 109 (E9).
Campbell, B., 1992. Comparison of Magellan measurements of surface roughness on Venus to topographic profiles of terrestrial basaltic lava flows. Abstr. Lunar Planet. Sci. Conf. 23, 201.
Campbell, Bruce A., 1995. Use and presentation of Magellan quantitative data in Venus mapping. US Department of the Interior, US Geological Survey.
Campbell, B.A., Campbell, D.B., 1992. Analysis of volcanic surface morphology on Venus from comparison of Arecibo, Magellan, and terrestrial airborne radar data. J. Geophys. Res. 97, 16,293. https://doi.org/10.1029/92JE01558.
Campbell, B.A., Rogers, P.G., 1994. Bell Regio, Venus: integration of remote sensing data and terrestrial analogs for geologic analysis. J. Geophys. Res. Planet 99 (E10), 21153–21171.
Campbell, D.B., Stacy, N.J.S., Newman, W.I., Arvidson, R.E., Jones, E.M., Musser, G.S., Schaller, C., 1992. Magellan observations of extended impact crater related features on the surface of Venus. J. Geophys. Res. Planet 97 (E10), 16249–16277.
Carter, L.M., Campbell, D.B., Campbell, B.A., 2004. Impact crater related surficial deposits on Venus: multipolarization radar observations with Arecibo. J. Geophys. Res. Planet 109 (E6).
Carter, L.M., Campbell, D.B., Campbell, B.A., 2006. Volcanic deposits in shield fields and highland regions on Venus: surface properties from radar polarimetry. J. Geophys. Res. Planet 111 (E6).
Chen, Allen, Lange, Rob, Ono, Hiro, Otero, Richard, Trosper, Jennifer, Villar, Gregory, 2017. Landing site engineering assessment, *Mars* 2020 Landing Site Workshop 3, Monrovia, California, February 8. https://trs.jpl.nasa.gov/handle/2014/47429.
Esposito, L.W., 2017. Venus In Situ Atmospheric and Geochemical Explorer (VISAGE): A Proposed New Frontiers Mission. In: Lunar and Planetary Science Conference, Vol. 48. LPI Contribution No. 1964, id.2444.
Florensky, C.P., Ronca, L.B., Basilevsky, A.T., Burba, G.A, Nikolaeva, O.V., Pronin, A.A., Trakhtman, A.M., Volkov, V.P., Zazetsky, V.V., 1977. The surface of Venus as revealed by Soviet Venera 9 and 10. GSA Bulletin 88 (11), 1537–1545. https://doi.org/10.1130/0016-7606(1977)88<1537:TSOVAR>2.0.CO;2.
Ford, John P., Plaut, Jeffrey J., Weitz, Catherine M., Farr, Tom G., Senske, David A., Stofan, Ellen R., Michaels, Gregory, Parker, Timothy J., Fulton, D., 1993. Guide to Magellan image interpretation. In: JPL Publication 93–24, NASA-CR-194340.
Garvin, J., Head, J., 1983. Radar roughness at Venus landing sites. Lunar Planet. Sci. Conf. 14, 235–236.
Garvin, J., Arney, G., Getty, S., Johnson, N., Kiefer, W., Lorenz, R., Ravine, M., Malespin, C., Webster, C., Campbell, B., Izenberg, N., Cottini, V., DAVINCI+ Mission engineering team (GSFC, LM, JPL, MSSS, LaRC, ARC, APL), 2020. DAVINCI+: Deep Atmosphere of Venus Investigation of Noble Gases, Chemistry, & Imaging, Plus, *52st LPSC, Abstract 2599*. https://www.hou.usra.edu/meetings/lpsc2020/pdf/2599.pdf. Accessed 1 Oct 2020.
Golombek, M., Rapp, D., 1997. Size-frequency distributions of rocks on Mars and Earth analog sites: implications for future landed missions. J. Geophys. Res. Planet 102 (E2), 4117–4129.
Golombek, M.P., Cook, R.A., Moore, H.J., Parker, T.J., 1997. Selection of the Mars Pathfinder landing site. J. Geophys. Res. 102 (E2), 3967–3988. https://doi.org/10.1029/96JE03318.

Golombek, M., Haldemann, A.F., Forsberg-Taylor, N., DiMaggio, E., Schroeder, R., Jakosky, B., Mellon, M., Matijevic, J., 2003a. Rock size-frequency distributions on Mars and implications for Mars Exploration Rover landing safety and operations. J. Geophys. Res. Planet 108 (E12).

Golombek, M.P., Grant, J.A., Parker, T.J., Kass, D.M., Crisp, J.A., Squyres, S.W., Haldemann, A.F.C., Adler, M., Lee, W.J., Bridges, N.T., Arvidson, R.E., Carr, M.H., Kirk, R.L., Knocke, P.C., Roncoli, R.B., Weitz, C.M., Schofield, J.T., Zurek, R.W., Christensen, P.R., Fergason, R.L., Anderson, F.S., Rice Jr., J.W., 2003b. Selection of the Mars Exploration Rover landing sites. J. Geophys. Res. 108, 8072. https://doi.org/10.1029/2003JE002074. E12.

Golombek, M., Grant, J., Kipp, D., Vasavada, A., Kirk, R., Fergason, R., Bellutta, P., Calef, F., Larsen, K., Katayama, Y., Huertas, A., Beyer, R., Chen, A., Parker, T., Pollard, B., Lee, S., Sun, Y., Hoover, R., Sladek, H., Grotzinger, J., Welch, R., Noe Dobrea, E., Michalski, J., Watkins, M., 2012. Selection of the Mars Science Laboratory Landing Site. *Space Sci.* Rev. 170, 641. https://doi.org/10.1007/s11214-012-9916-y.

Helbert, J., Dyar, M.D., Izenberg, N.R., Ghail, R.C., Garvin, J.B., Byrne, P.K., Smrekar, S. E., Gilmore, M., Widemann, T., Beauchamp, P.M., Shaji, N., Zasova, L., 2020. Why We Need a Long-Term Sustainable Venus Program, *LPSC 51*, Abstract #1427. https://www.hou.usra.edu/meetings/lpsc2020/pdf/1427.pdf accessed 1 Oct 2019.

Hensley, S., Smrekar, S., Nunes, D., Mueller, N., Helbert, J., Mazarico, E., the VERITAS Science Team, 2016. VERITAS: Towards the Next Generation of Cartography for the Planet Venus, *47th LPSC Conference*, Houston, TX, Abstract #1965. https://www.hou.usra.edu/meetings/lpsc2016/pdf/1965.pdf. Accessed 1 Oct 2019.

Ivanov, M.A., Head, J.W., 2011. Global geological map of Venus. Planet. Space Sci. 59 (13), 1559–1600.

Ivanov, M.A., et al., 2017a. The nature of terrains of different types on the surface of Venus and selection of potential landing sites for a descent probe of the Venera-D Mission. Sol. Syst. Res. 51 (1), 1–19.

Ivanov, M.A., et al., 2017b. Estimates of abundance of the short-baseline (1-3 meters) slopes for different Venusian terrains using terrestrial analogues. Sol. Syst. Res. 51 (2), 87–103.

Kratter, K.M., Carter, L.M., Campbell, D.B., 2007. An expanded view of Lada Terra, Venus: new Arecibo radar observations of Quetzalpetlatl Corona and surrounding flows. J. Geophys. Res. Planet 112 (E4).

O'Rourke, J., Treiman, A., Arney, G., Byrne, P., Carter, L., Dyar, D., Head III, J., Gray, C., Kane, S., Kiefer, W., McGouldrick, K., Montesi, L., Russell, C., Smrekar, S., 2019. Venus Goals, Objectives, and Investigations. https://www.lpi.usra.edu/vexag/.

Pettengill, G.H., Ford, P.G., Brown, W.E., Kaula, W.M., Keller, C.H., Masursky, H., McGill, G.E., 1979. Pioneer Venus radar mapper experiment. Science 203 (4382), 806–808.

Pettengill, Gordon H., Ford, Peter G., Wilt, Robert J., 1992. Venus surface radiothermal emission as observed by Magellan. J. Geophys. Res. Planet 97 (E8), 13091–13102.

Saunders, R.S., Spear, A.J., Allin, P.C., Austin, R.S., Berman, A.L., Chandlee, R.C., Clark, J., et al., 1992. Magellan mission summary. J. Geophys. Res. Planet 97 (E8), 13067–13090.

Seiff, A., Schofield, J.T., Kliore, A.J., Taylor, F.W., Limaye, S.S., Revercomb, H.E., Sromovsky, L.A., Kerzhanovich, V.V., Moroz, V.I., Marov, M. Ya, 1985. Models of the structure of the atmosphere of Venus from the surface to 100 kilometers altitude. Adv. Space Res. 5 (11), 3–58.

Shepard, M.K., Campbell, B.A., Bulmer, M.H., Farr, T.G., Gaddis, L.R., Plaut, J.J., 2001. The roughness of natural terrain: a planetary and remote sensing perspective. J. Geophys. Res. 106 (E12), 32777–32795.

Tyler, G. Leonard, Ford, Peter G., Campbell, Donald B., Elachi, Charles, Pettengill, Gordon H., Simpson, Richard A., 1991. Magellan: Electrical and Physical Properties of Venus' Surface. Science 252 (5003), 265–270. https://doi.org/10.1126/science.252.5003.265.

Ulaby, F.T., Moore, R.K., Fung, A.K., 1982. Microwave Remote Sensing: Active and Passive, Vol. II. Radar Remote Sensing. Addison-Wesley, Reading, Massachusetts.

Vasavada, A.R., Chen, A., Barnes, J.R., Burkhart, P.D., Cantor, B.A., Dwyer-Cianciolo, A. M., Fergason, R.L., Hinson, D.P., Justh, H.L., Kass, D.M., Lewis, S.R., Mischna, M.A., Murphy, J.R., Rafkin, S.C.R., Tyler, D., Withers, P.G., 2012. Assessment of environments for Mars science laboratory entry, descent, and surface operations. Space Sci. Rev. 170, 793–835. https://doi.org/10.1007/s11214-012-9911-3.

Weitz, Catherine M., Basilevsky, Alexander T., 1993. Magellan observations of the Venera and Vega landing site regions. J. Geophys. Res. Planet 98 (E9), 17069–17097.